Expression of human CEACAMs promotes inflammation and organ damage during systemic *Candida albicans* infection in mice

Esther Klaile[1, 2*], Mario M. Müller[2, 3], Johannes Sonnberger[2, 4], Anne-Katrin Bothe[2, 5], Saskia Brehme[2], Juliet Ehrenpfordt[2], Tilman E. Klassert[6, 7], Sabina Kuhn[2], Kristina Dietert[8, 9], Olivia Kershaw[9], Jan-Philipp Praetorius[10, 11], Marc Thilo Figge[10, 12], Torsten Bauer[13], Andreas Gebhardt[13], Gita Mall[14], Ilse D. Jacobsen[15, 16], Hortense Slevogt[17, 6]

[1]Center for Clinical Studies, Jena University Hospital, Jena, Germany

[2]Host Septomics Group, Centre for Innovation Competence (ZIK) Septomics, Jena University Hospital, Jena, Germany

[3]Functional Proteomics, Jena University Hospital, Jena, Germany

[4]Microbial Pathogenicity Mechanisms, Leibniz Institute for Natural Product Research and Infection Biology Hans Knöll Institute (HKI), Jena, Germany

[5]Dynamic42 GmbH, Jena, Germany

[6]Respiratory Infection Dynamics, Helmholtz Centre for Infection Research - HZI Braunschweig, Braunschweig, Germany

[7]German Center for Lung Research (DZL), BREATH, Hannover, Germany

[8]Veterinary Centre for Resistance Research (TZR), Freie Universität Berlin, Berlin, Germany

[9]Institut für Tierpathologie, Freie Universität Berlin, Berlin, Germany

[10]Applied Systems Biology, Leibniz institute for natural Product Research and infection Biology – Hans Knöll institute (HKI), Jena, Germany

[11]Faculty of Biological Sciences, Friedrich Schiller University Jena, Jena, Germany

[12]Institute of Microbiology, Faculty of Biological Sciences, Friedrich Schiller University Jena, Jena, Germany

[13]Department of Pneumology, Lungenklinik Heckeshorn, Helios Klinikum Emil von Behring, Berlin, Germany

[14]Institut für Rechtsmedizin, Jena University Hospital, Jena, Germany

[15]Research Group Microbial Immunology, Leibniz Institute for Natural Product Research and Infection Biology Hans Knöll Institute (HKI), Jena, Germany

[16]Institute of Microbiology, Friedrich Schiller University Jena, Jena, Germany

[17]Department of Respiratory Medicine and Infectious Diseases, Hannover Medical School, Germany

*** Correspondence:** Esther Klaile esther.klaile@med.uni-jena.de

Keywords: carcinoembryonic antigen-related cell adhesion molecule 6 (CEACAM6), *Candida albicans*, candidiasis mouse model, bone marrow-derived neutrophil (BMN), bone marrow-derived monocyte (BMM), bone marrow-derived macrophage (BMDM)

Running title: CEACAM6+ cells exacerbate candidiasis
Manuscript Length: 4332 words
Number of Figures and Tables: 8

Abstract

Invasive candidiasis is a fungal infection characterized by a high mortality rate. CEACAM family receptors play a crucial role in regulating innate responses of both leukocytes and epithelia. Human CEACAM3, CEACAM5 and CEACAM6 receptors recognize *C. albicans* and are expressed in transgenic CEABAC10 mice. In a murine *C. albicans* infection model, CEABAC10 mice exhibited a shortened survival period attributed to an early cytokine storm, an exacerbated acute phase response, and heightened systemic inflammation compared to their wild-type littermates. The livers and kidneys of CEABAC10 mice displayed intensified purulent necrotizing inflammation, accompanied by increased infiltration of neutrophils and macrophages. Our *in vivo* and *in vitro* data indicated that the expression of CEACAM6 on monocytes of CEABAC10 mice caused the elevated cytokine levels and the subsequent exacerbation of the acute phase response upon *C. albicans* infection, resulting in decreased survival.

1 Introduction

The fungal pathogen *Candida albicans* is a predominant cause of human *Candida* bloodstream infections, associated with elevated mortality rates[1, 2]. The incidence of systemic candidiasis is on the rise, particularly among patients with high-risk factors such as prior antibiotic exposure, chemotherapy, hematopoietic stem cell transplantation, prolonged intensive care requirements due to other medical conditions, and the use of central venous catheters[3].

Host defense against systemic candidiasis relies on the crucial role of myeloid phagocytes, including neutrophils, inflammatory monocytes, and tissue-resident macrophages[2]. The initial phase of their interaction with the fungus involves the fundamental step of fungal recognition, which mounts the inflammatory response against the invading fungus, orchestrates pathogen uptake and systemic inflammatory responses during blood stream infections.

In addition to pattern recognition receptors[4, 5], *C. albicans* is recognized by members of the human CEACAM receptor family, namely CEACAM1, CEACAM3, CEACAM5, and CEACAM6[6]. CEACAM1 and CEACAM3 are modulatory receptors that signal via their intracellular immunoreceptor tyrosine-based inhibitory motif (ITIM) and immunoreceptor tyrosine-based activation motif (ITAM), respectively. CEACAM5 and CEACAM6 are GPI anchored and organized in membrane microdomains[7, 8]. The well-described immunoregulatory function of CEACAM1 is complemented by the impact of CEACAM3, CEACAM5, and CEACAM6 on immune reactions across a diverse array of cell types[9, 10, 11, 12, 13]. *In vitro* data indicate immunoregulatory roles for human CEACAM1 and CEACAM6 in the innate immune response of human intestinal epithelial cells and human neutrophils triggered by *C. albicans* stimulation[6, 14]. However, the expression of human CEACAM1 in transgenic mice had no discernible effect on their susceptibility to systemic candidiasis or on *C. albicans* colonization/dissemination[15].

Similar to its human homolog, mouse CEACAM1 serves as a receptor for host-specific pathogens such as the murine hepatitis virus (MHV)[16], and possesses regulatory functions in immune responses across diverse cell types, both *in vivo* and *in vitro*[17, 18]. However, mouse CEACAM1 does not bind to *C. albicans* cell surface structures[6]. Notably, mice lack the homologous genes for CEACAM3, CEACAM5, and CEACAM6 receptors[19].

Chan and Stanners developed CEABAC10 mice transgenic for human CEACAM3, CEACAM5, CEACAM6, and CEACAM7, including the human promotor region[20]. The

extensive epithelial expression of CEACAM5 and CEACAM6 on the surface of various mucosal tissues in CEABAC10 mice, including the intestinal tract, closely mirrors their expression in humans[20]. While CEACAM5 is specifically expressed on apical membranes of epithelial cells, CEACAM6 is also present on immune cells, including neutrophils, alongside the neutrophil-specific CEACAM3[20]. Notably, CEACAM7 does not bind to *C. albicans* and is selectively expressed in a limited number of highly differentiated epithelial cells in the colon[6, 20]. The CEABAC10 mouse model is widely employed for analyzing CEACAM receptor functions in the host's response to infections with human pathogens. It provided crucial insight into the role of CEACAM6 in conjunction with adhering-invasive *E. coli* (AIEC) in Crohns Disease pathology *in vivo*[21, 22], and has contributed valuable information regarding the involvement of CEACAM receptors in the neutrophil response to *Neisseria gonorrhea in vitro*[23].

In the present study, we used the CEABAC10 mouse model to investigate the impact of CEACAM3, CEACAM5, and CEACAM6 on disseminated candidiasis *in vivo* [15, 24, 25]. The presence of CEACAMs led to severe infection pathology, a heightened IL-6-mediated acute phase response, and early death in candidemic CEABAC10 mice. Through *in vitro* experiments employing primary bone marrow-derived myeloid cells, we found that CEACAM3 expression did not affect inflammatory responses, and we identified CEACAM6$^+$ classical monocytes and resident macrophages as the cell populations responsible for the hyperinflammatory response to systemic *C. albicans* infection in CEABAC10 mice. These findings suggest that CEACAM6 may play a previously unknown role in the inflammatory response of mononuclear phagocytes during systemic candidiasis.

2 Results

2.1 Human CEACAM-transgenic CEABAC10 mice are more susceptible to systemic candidiasis

In an intravenous infection model using two different infectious doses, our results showed a marked increase in susceptibility to systemic candidiasis and earlier death of CEABAC10 mice (CEA) compared to their wild-type (WT) littermates (Figure 1a, Figure S1). Proinflammatory cytokine responses were indistinguishable at 24 h post infection (p.i.) in WT and CEABAC10 mice, but at 72 h p.i., CEABAC10 mice exhibited significantly elevated serum levels of IL-6, TNFα, GM-CSF, IL-2, IL-4, CXCL10, and VEGF, indicative of an exacerbated inflammatory response (Figure 1b-d, Figure S2). Moreover, CEABAC10 mice displayed a diminished count of neutrophils and monocytes in their blood 24 h p.i., suggesting an enhanced recruitment of peripheral leukocytes into infected tissue (Figure 1e, f). Analysis of bone marrow cell populations revealed no disparities in hematopoiesis between CEABAC10 and WT mice during infection (Figure S3). Additionally, CEABAC10 mice exhibited a significant reduction in platelet numbers 24 h p.i., along with enlarged platelet volumes 72 h p.i., suggesting increased consumption and subsequent replenishment (Figure S4), indicative of increased bleeding and thrombosis typical for septic progression[26].

To explore the inflammatory response and heightened susceptibility of CEABAC10 mice to systemic candidiasis in more detail, we conducted an analysis of serum glycoproteome changes (Figure 2). Principal component analysis revealed that samples from mice injected with PBS separated from those infected with *C. albicans* at 24 h and 72 h, respectively. In addition, CEABAC10 sera notably diverged from WT samples at 72 h p.i. (Figure 2a).

Consistent with the principal component analysis, the comparison between PBS control-treated and *C. albicans*-infected WT mice revealed 29 and 103 differentially expressed serum

128 glycoproteins at 24 h p.i. and 72 h p.i., respectively (Figures 2b, c and Tables S1, S2). No
129 significant differences in serum glycoprotein abundance were detected between PBS-treated
130 WT and CEABAC10 control mice and between WT and CEABAC10 animals 24 h p.i.
131 (Figure 2d, e). In contrast, at 72 h p.i., the serum glycoprotein composition between WT and
132 CEABAC10 mice revealed significant changes. Overall, 51 glycoproteins were differentially
133 abundant in serum with 14 showing higher abundance in CEABAC10 mice and 37 elevated in
134 WT animals (Figure 2f and Table S5). Pathway analysis with Qiagens IPA software revealed
135 a robust activation of the acute phase response in *C. albicans*-infected WT animals at 24 h p.i.
136 that further progressed at 72 h p.i., accompanied with changes in proteins associated with the
137 activity of the coagulation and complement system and LXR/RXR and FXR/RXR responses
138 (Figures 2g, h and Tables S3, S4). In comparison to WT animals, CEABAC10 mice revealed
139 a stronger acute phase response at 72 h p.i., and alterations of coagulation, complement und
140 prothrombin pathways (Figure 2i, Table S6). Consequently, the serum glycoproteome data
141 suggest an exacerbation of the systemic septic response in CEABAC10 mice initiated by
142 *C. albicans* infection.

143 **2.2 Infected kidneys of CEABAC10 mice display pronounced purulent necrotizing**
144 **nephritis 72 h p.i.**

145 To further explore disease progression, we next investigated inflammatory responses in
146 various organs after *C. albicans* infection in more detail. The kidney is the main target organ
147 in the murine intravenous model of systemic candidiasis[27]. Examination of hematoxylin-eosin
148 (HE)-stained kidney sections revealed renal inflammation 24 h p.i. in both WT and
149 CEABAC10 mice (Figure 3a, c, e-h). Subsequently, from 24 h to 72 h p.i., the extent of
150 kidney inflammation escalated in CEABAC10 but remained relatively stable in WT mice
151 (Figure 3b, d, e-h). This was evidenced by the higher inflammation score (Figure 3e), the
152 increased number of inflammatory foci (Figure 3f), and the larger total area of inflamed tissue
153 (Figure 3h). Interestingly, the mean area of inflammatory foci remained similar between WT
154 and CEABAC10 kidneys (Figure 3g). The heightened degree of kidney inflammation in
155 infected CEABAC10 mice was further underscored by significantly higher levels of pro-
156 inflammatory cytokines (IL-6, IL-1β, Figure 3i-j; IL-1α, Figure S5), chemo-attractants
157 (CCL2/MCP-1, Figure 3k; CCL3/MIP1 α, CXCL1/KC, Figure S5), and growth factors
158 (bFGF, GM-CSF, Figure S5) in CEABAC10 kidney homogenates at 72 h p.i.

159 In the kidneys of infected CEABAC10 mice, immune cell populations exhibit a notable
160 relative decrease in NK cells (Figure S6c), but a significant relative increase in neutrophils
161 (Figure 3l) at 72 h p.i.. There was an observed increase in fungal burden, measured as CFU
162 (Figure 3m), visualized by histology (Figure 3n, o), and quantified by automated image
163 analysis of the area covered by fungi (Figure S6f). Also, hyphal growth was increased in
164 CEABAC10 kidneys (Figure 3n, o, p, Figure S6g). Immunohistochemistry (IHC) showed that
165 CEACAM6 was exclusively present in neutrophils, monocytes, and macrophages in
166 CEABAC10 kidney sections (Figure 3q, r). Due to its high glycosylation[28], CEACAM6 is
167 proteolytically stable, and its presence was detectable in areas with high counts of
168 damaged/deceased immune cells at 72 h p.i., particularly on neutrophils (Figure 3q, r). IHC
169 analysis of consecutive sections for neutrophil elastase (Figure 3s), detectable only in viable
170 neutrophils, indicated that dead cells outnumbered viable neutrophils. Consequently, the
171 quantification of viable neutrophils by flow cytometry likely underestimated the extent of
172 increased neutrophil recruitment into inflamed CEABAC10 kidney tissue.

173

174 **2.3 The expression of human CEACAM3 and CEACAM6 does not alter the response**
175 **of bone marrow-derived neutrophils to *C. albicans in vitro***

176 Neutrophils play a pivotal role in the host response against *C. albicans*[3], yet they also
177 contribute to pathogenesis by inflammation-driven tissue damage[29, 30]. The enhanced
178 recruitment of neutrophils, coupled with a higher fungal burden and increased numbers of
179 inflammatory foci in the kidneys of CEABAC10 mice, implied a potential reduction in the
180 antifungal activity of these cells. Thus, we sought to investigate the response of bone marrow-
181 derived neutrophils (BMN) to *C. albicans* infection *in vitro*. CEABAC10 BMN express
182 CEACAM3 and CEACAM6 on their cell surface (Figure 4a, b), both of which regulate
183 various human neutrophil functions such as pathogen recognition and uptake, modulation of
184 apoptosis, and adhesion to endothelial cells[14, 31, 32, 33]. Given that CEACAM6 is also present in
185 primary/azurophilic granules of human neutrophils and can be de-granulated to increase the
186 cell surface expression level upon neutrophil activation[31], we assessed the expression of
187 human CEACAM receptors on transgenic BMN by flow cytometry. Upon stimulation of
188 CEABAC10-derived BMNs with *C. albicans*, a significant increase of both, human
189 CEACAM3 and CEACAM6, on BMN cell surfaces was observed (Figure 4c, d), indicating
190 similar behavior of the receptors in transgenic murine neutrophils.

191 The integrin CD11b/CD18 (CR3, αMβ2, MO-1, Mac-1) plays a crucial role in mediating
192 neutrophil extravasation. CR3 can be activated and upregulated upon human neutrophil
193 activation and ligation of CEACAM3 and CEACAM6[33]. Stimulation of BMNs with
194 *C. albicans* led to a similar increase of cell surface-associated CD11b in both WT and
195 CEABAC10 cells (Figure 4e), indicating similar activation states of BMNs after *C. albicans*
196 recognition. Furthermore, no discernible differences related to spontaneous and *C. albicans*-
197 induced neutrophil death, binding and phagocytosis of *C. albicans*, or fungal killing were
198 observed in isolated BMNs from WT and CEABAC10 mice *in vitro* (Figure 4f-h). While a
199 slightly higher basal level of reactive oxygen species (ROS) was detected in CEABAC10
200 BMNs, the quantities of ROS induced by *C. albicans* were comparable between WT and
201 CEABAC10 BMNs (Figure 4i). Also, there was no significant difference in the release of
202 proinflammatory CXCL1 (KC), but CEABAC10 BMNs exhibited a less variable and lower
203 release of the degranulation marker myeloperoxidase (Figure 4j, k).

204 In summary, the expression of human CEACAM3 and CEACAM6 did not fundamentally
205 alter the interaction of BMNs with *C. albicans in vitro*. However, the microenvironment of
206 inflamed tissues may well influence neutrophil behavior *in vivo*, and the elevated numbers of
207 neutrophils likely contribute to heightened inflammation and tissue damage.

208 **2.4 CEABAC10 mice develop acute hepatic coagulation necroses, purulent necrotizing**
209 **hepatitis, purulent splenitis, and brain hemorrhage during systemic candidiasis**

210 Following intravenous infection of WT mice, *C. albicans* is typically cleared from the liver
211 over time without causing visible tissue alterations[27], a trend also observed in our experiments
212 (Figure 5a, c). In contrast, at necropsy 72 h p.i., prominent white areas were evident on the
213 livers of 15 out of 18 CEABAC10 (Figure 5b, c). Histologically, these alterations correlated
214 with multifocal acute coagulation necroses with immune cell infiltrations (Figure 5d-f).
215 Notably, these lesions were strictly vascular associated, predominantly periportally localized,
216 and nearly exclusive to CEABAC10 livers (Figure 5g). The onset of coagulation necroses and
217 immune cell infiltrations was detected microscopically as early as 24 h p.i., intensifying in
218 numbers and size by 72 h p.i. (Figure 5g), when they became macroscopically visible.
219 Additionally, acute purulent necrotizing hepatitis was observed in 6 out of 11 CEABAC10
220 mice 72 h p.i., contrasting with the absence of such findings in WT animals (Figure 5h).

221 The inflammatory nature of these lesions was evident through the higher relative numbers of
222 neutrophils and macrophages detected by flow cytometry in livers of CEABAC10 mice
223 (Figure 5i, j), accompanied by elevated levels of pro-inflammatory cytokines and chemokines
224 in liver homogenates (IL-6, CCL2/MCP-1, CCL3/MIP-1α, and CXCL10/IP-10; Figure 5k-m,
225 Figure S9). While the proportion of monocytes among hepatic immune cells was comparable
226 between WT and CEABAC10 mice, there was a tendency towards a relative reduction of NK
227 cell, T cell, and B cell numbers in CEABAC10 livers 72 h p.i. (Figure S10). Despite the
228 heightened inflammation in the livers of CEABAC10 mice, the total fungal burden in the liver
229 tissue was comparable to WT animals (Figure 5n). Similar to the kidneys, only neutrophils,
230 along with macrophages and monocytes stained positive for CEACAM6 (Figure S10), and
231 live, neutrophil elastase (NE)-positive granulocytes were outnumbered by dead CEACAM6-
232 posive neutrophils and macrophages 72 h p.i. (Figure S10).

233 In addition to the liver pathology, severe purulent splenitis was also observed in 8 out of 11
234 CEABAC10 mice at 72 h p.i., a condition only detected in 1 out of 7 WT mice (Figure 5r).
235 Despite this discrepancy in pathology, the composition of immune cell populations and fungal
236 load were not significantly different in spleens of infected WT and CEABAC10 mice (Figure
237 S12, Figure 5s).

238 Interestingly, four out of 18 CEABAC10 mice exhibited brain hemorrhage at 72 h p.i. at
239 necropsy, which was not seen in any of the 14 WT mice at 72 h (Figure S14). No difference in
240 the severity of encephalitis was observed between the two genotypes, although CEABAC10
241 brains displayed higher fungal burdens and higher hyphae scores (Figure S14). Similar to
242 other organs, CEACAM6 expression in the brain was restricted to neutrophils and some
243 macrophages (Figure S14), and dead CEACAM6-positive neutrophils and macrophages
244 outnumbered viable, neutrophil elastase (NE)-positive granulocytes (Figure S14).

245 2.5 CEACAM6 expression on monocytes, but not macrophages, leads to increased 246 cytokine production in response to *C. albicans*

247 The activation of leukocytes induces an increased expression of CEACAMs on their surface[31].
248 In evaluating the activation of myeloid cells following systemic candidiasis, we focused on
249 assessing the expression of CEACAM6 that is expressed by neutrophils, monocytes, and
250 macrophages in CEABAC10 mice. The proportion of CEACAM6$^+$ neutrophils increased from
251 approximately 80% to nearly 100% at 72 h p.i. in kidney, liver, and spleen (Figure 6a, d, g).
252 While CEACAM6$^+$ monocytes were scarce in PBS control mice, their numbers increased to
253 approximately 50% of the total monocyte population in the kidney, liver, and spleen at 72 h
254 p.i. (Figure 6b, e, h).

255 In macrophages, the CEACAM6$^+$ subpopulation remained remarkably stable during infection
256 in kidneys and spleen. Approximately 6% of all macrophages in the kidneys (Figure 6c) and
257 around 10% in the spleen (Figure 6i) were CEACAM6-positive cells. Interestingly, a
258 contrasting scenario unfolded in the liver: Here, a substantial proportion of CEACAM6$^+$
259 macrophages (approximately 40%) was observed in PBS-treated control animals (Figure 6f).
260 However, this population dropped below 10% within 24 h p.i. and remained low at 72 h p.i.
261 (Figure 6f). One plausible explanation for the reduced proportion of CEACAM6$^+$
262 macrophages is macrophage cell death, as only viable cells were quantified by flow
263 cytometry, and a substantial number of CEACAM6$^+$ dead cells, including macrophages, were
264 visible in immunohistochemistry (Figure 5p).

265 Since the expression of CEACAM3 and CEACAM6 did not influence BMN interaction with
266 and response to *C. albicans*, we postulated that CEACAM6$^+$ transgenic macrophages and

monocytes are crucial for the heightened inflammatory response observed in CEABAC10 mice during systemic candidiasis. We therefore studied responses to *C. albicans* infection in transgenic and WT bone marrow-derived macrophages (BMDMs) *in vitro*. The majority of BMDMs stained positive for CEACAM6 (Figure 7a, b). While phagocytosis of *C. albicans* was slightly but significantly higher in CEABAC10 BMDMs (Figure 7c), *C. albicans*-induced macrophage cell death was comparable between both WT and CEABAC10 BMDM (Figure 7d). These findings suggest that macrophage expression of CEACAM6 *per se* is not the primary factor responsible for the substantial number of dead hepatic macrophages observed after infection *in vivo* (Figure 6f). Moreover, the release of the pro-inflammatory cytokines IL-1β, IL-6, and TNFα was not significantly affected by CEACAM6 expression in BMDMs (Figure 7d-f).

In CEABAC10 bone marrow-derived monocytes (BMMs), only the classical subset (CD62L$^+$/CD11c$^-$), and not the non-classical subset (CD62L$^-$/CD11c$^+$) expressed CEACAM6 on the surface (Figure 8a-d). Nevertheless, this mixed population of CEABAC10-derived BMMs with >50% CEACAM6$^+$ cells demonstrated a significantly increased production of IL-6 and CCL2/MIP-1α after *C. albicans* infection compared to WT BMMs, aligning with the higher cytokine production observed in mouse tissues *in vivo*. In contrast, the amount of secreted TNFα and IL-1β after infection was comparable in both WT- and CEABAC10-derived BMMs irrespective of CEACAM6 expression.

The identification of a specific subset of macrophages expressing CEACAM6 in the livers of transgenic mice aligns with the results from the analysis of human liver sections, where a substantial portion of resident CD68$^+$ macrophages[34] was also positive for CEACAM6 (Figure S17). Additionally, closely mirroring this pattern, about one-third of CD169$^+$ alveolar macrophages[35], as detected via flow cytometry in cell pellets from human bronchoalveolar lavage samples, were CEACAM6-positive (Figure S18). In contrast to CEABAC10 monocytes (Figure 6b, 3, h), peripheral monocytes isolated from fresh blood of healthy human volunteers showed no detectable surface expression of CEACAM6 (Figure S19).

3 Discussion

CEACAM family receptors play a crucial role in regulating immune functions during infections and cancer[8, 28, 36]. CEACAM1 is recruited and activated by bacterial and viral pathogens to suppress immune responses[8, 28, 36]. Conversely, CEACAM6 primarily functions as an adhesin for human pathogens like AIEC, *Neisseria spec.*, and *Acinetobacter baumannii*, permitting colonization and invasion of cells and tissues without directly affecting host responses[10, 13, 21]. CEABAC10 mice[20] serve as a valuable model for studying interactions of human pathogens with CEACAM3, CEACAM5, and CEACAM6 both *in vivo* and *in vitro*[13, 21, 22, 23, 37, 38]. In this study, we explore the impact of their expression on the host response to systemic candidiasis.

CEABAC10 mice exhibited a heightened susceptibility and accelerated mortality in response to systemic *C. albicans* infection. This increased vulnerability can be at least partially attributed to an exacerbated systemic immune response, characterized by elevated cytokine levels and an intensified acute phase response, in line with the contribution of progressive sepsis to death of mice systemically infected with *C. albicans*[39]. In addition, increasing fungal burden in the kidneys as the primary target organ[27] leads to renal failure[39]. Here, we found that CEABAC10 kidneys were severely affected at 72 h p.i. with increased inflammation and fungal burden, indicating that both augmented immunopathology and reduced ability to control fungal growth contributed to the increased susceptibility of transgenic mice.

313 Neutrophils are crucial for the host defense against systemic candidiasis[3], and they express
314 functional CEACAM3[23] and CEACAM6[8, 28]. Thus, functional impairment of transgenic
315 neutrophils would explain the higher fungal burden, and increased recruitment of neutrophils
316 in CEABAC10 mice in response to the high fungal load likely resulted in increased renal
317 injury[40, 41]. However, we found no evidence of reduced anti-fungal activity of CEABAC10
318 BMNs *in vitro*. Possibly, neutrophil behavior *in vivo* is influenced by infection-specific
319 alterations of the tissue environment that were absent in BMN experiments *in vitro*. Our
320 serum glycoproteome analysis showed markedly dysregulated levels of several matrix
321 proteins and secreted/shed immunoregulatory receptors and enzymes in CEABAC10 serum,
322 including the key enzyme for heparan sulfate chain initiation, EXTL2. In mouse models for
323 vulvovaginal candidiasis, heparan sulfate in the vaginal environment of susceptible mice
324 serves as a competitive ligand for Mac-1 on neutrophils, effectively rendering the neutrophils
325 unable to bind to *Candida* to initiate killing[42]. Pathway analysis of the serum glycoproteomes
326 of WT and CEABAC10 mice 72 h p.i. further identified a dysregulation of the LXR/RXR
327 activation, which regulates neutrophil functions[43] as well as monocyte/macrophage cytokine
328 release[44, 45].

329 Interestingly, CEABAC10 livers also showed clear inflammatory changes and tissue damage.
330 This was unexpected because in WT mice, liver infection is normally controlled by the
331 murine immune system, and tissue architecture is preserved without evident inflammatory
332 changes, except for the transient accumulation of both neutrophils and mononuclear
333 phagocytes[27]. Enhanced numbers of monocytic phagocytes can lead to tissue damage, as
334 shown by mouse liver injury exacerbated by CCL2-mediated monocyte/macrophage
335 recruitment[46]. In fact, our data suggested that CEABAC10 monocytes and macrophages were
336 the driving force behind the observed systemic inflammation and organ damage, acutely
337 affecting the liver. Recently, an increasing number of publications have focused on the role of
338 monocytic phagocytes in systemic candidiasis[3, 47]. Monocytes closely control the early host
339 reaction to *C. albicans* infection, primarily by secretion of various cytokines and chemokines,
340 including IL6 and CCL2/MIP-1α[48, 49, 50]. *Candida*-stimulated CEABAC10 bone marrow-
341 derived monocytes released substantially increased amounts of IL-6 and CCL2/MIP-1α,
342 consistent with their marked increase *in vivo* in infected CEABAC10 mice.

343 As the primary immune cells in naive tissues, tissue-resident macrophages are essential for
344 innate host defense against *C. albicans* infection[47]. CCL2 further enhances monocyte
345 recruitment to inflammatory sites, where they differentiate into macrophages[47, 51], as we found
346 in CEABAC10 livers 72 h p.i. CEABAC10 liver macrophages showed a contrasting behavior
347 with the loss of all CEACAM6$^+$ macrophages within 24 h p.i. and a strongly increased total
348 number of CEACAM6$^-$ macrophages. Regrettably, bone marrow-derived CEABAC10
349 macrophages were not a useful tool to study the role of macrophages during *Candida*
350 infection, probably due to the marked heterogeneity of macrophage populations as a function
351 of their microenvironment, as reviewed in detail previously[3, 47, 52]. However, in a CX3CR1
352 knock-out mouse model, the dysfunction of tissue macrophages was associated with a higher
353 fungal load in kidneys, higher neutrophil counts in kidneys, renal failure, and shortened
354 survival[53]. As in most murine studies of systemic *C. albicans* infection, the liver was not
355 further analyzed in this study[53] as it is usually not severely affected[27].

356 In CEABAC10 mice, the liver as key integrator of microbial responses[54] was likely central to
357 the exacerbation of sepsis progression via enhanced activation of the acute phase response
358 elicited by the increased levels of monocyte-derived IL-6. During microbial infection, IL-6
359 induces the liver to switch from tolerogenic towards immunogenic responses and initiate the
360 production of acute-phase proteins[54, 55]. In mice as well as in human patients, serum levels of
361 IL-6 are closely related to the severity and outcome of sepsis[56, 57]. In fact, IL-6 is the major

362 factor inducing a systemic inflammatory response syndrome in mouse models of sepsis[58],
363 furthered by inflammation and coagulation that promote organ dysfunction[26].

364 The rapid septic progression in CEABAC10 mice driven by the liver may have obscured
365 further roles of CEACAM6 receptors on monocytes and tissue macrophages in other organs[59].
366 For example, CEABAC10 brains showed increased fungal burden and hemorrhage.
367 *C. albicans* enters the brain by damaging the blood-brain-barrier[60], and microglia promote the
368 recruitment of neutrophils to the brain, which mediate fungal clearance[60, 61]. Further studies
369 will be needed to address the possible role of CEACAM6 expression on microglia and other
370 immune cells that may further impair blood vessel permeability.

371 This study confirms the results of our previous research on human neutrophils[14], which
372 showed that CEACAM6 expression plays a role in enhancing the responses triggered by other
373 receptors upon *C. albicans* infection rather than directly initiating a response. While
374 CEACAM1 shows very similar behavior to CEACAM6 in response to *C. albicans* infection
375 on human neutrophils[14], mice transgenic for human CEACAM1 show no difference in their
376 response to systemic candidiasis compared to their WT littermates[15]. Our data show that in
377 human neutrophils, CEACAM6 can influence different pattern recognition receptor pathways,
378 including Toll-like receptor (TLR), NOD-like receptor, and c-type lectin receptor signaling.
379 However, results from TLR2- and TLR-4-deficient mice infected with *C. albicans* remain
380 controversial, and in the consequences of TLR knock out for survival and fungal burden
381 depend on the genetic background, fungal strain, and infection dose[62]. Therefore, it remains
382 unclear if TLR interference by CEACAM6 might contribute to the increased susceptibility of
383 CEABAC10 mice. Dectin-1 deficiency renders mice susceptible to *C. albicans* infection due
384 to impaired neutrophil, monocyte, and macrophage recruitment and responses, including
385 impaired cytokine release, after infection even in the presence of opsonins[63]. This is in stark
386 contrast to increased recruitment of leucocytes and immunopathology observed with
387 CEABAC10 mice, making it unlikely that interference of CEACAM6 with Dectin-1 signaling
388 contributed to the observed phenotype.

389 Because of the intravenous route of infection used in this study, we believe that CEACAM6
390 expression on myeloid cells, particularly monocytes and monocyte-derived cells, rather than
391 mucosal CEACAM expression, lead to the exacerbated systemic inflammatory response
392 syndrome found in CEABAC10 mice. While there are some early publications indicating the
393 expression of CEACAM6 (also named CD66c, NCA-50/90, non-specific cross-reacting
394 antigen) on human monocytic cells and tissue macrophages[64, 65, 66], we were only able to
395 verify the expression of CEACAM6 in human tissue macrophages. The role of CEACAM6$^+$
396 mononuclear phagocytes remains to be further elucidated in primary human cells. Also, the
397 possibility of CEACAM6$^+$ monocyte subpopulations in systemically infected or septic
398 patients should be further explored.

399 4 Materials and Methods

400 4.1 *Candida albicans* strain and culture

401 *Candida albicans* Berkhout strain SC5314 was used for all experiments and was grown as
402 described[15]. In some cases, germ tubes were induced as described[15].

403 For FITC labelling, 10×10^7 yeast cells were suspended in 10 ml carbonate buffer (pH 9.5;
404 70% of sodium bicarbonate, 30% of sodium carbonate) and 100 µl of a FITC stock solution
405 (10 mg/ml in PBS) and incubated for one hour at 23°C, 150 rpm in the dark. Labeled yeast
406 cells were washed twice with PBS.

407 **4.2 Mouse strains**

408 FVB mice transgenic for the human CEACAM3, 5, 6, and 7 gene, CEABAC10[20], were
409 crossed into the C57BL/6NRj background using Speed Congenics. The status of the
410 background was supervised by GVG Genetic Monitoring (Leipzig, Germany). Mice were
411 bred heterozygous and a minimum of 12 backcrosses were performed prior to the first
412 experiment. The genotypes (CEABAC10+/- or wild type) were determined by PCR analysis
413 of tail biopsies using the following primer pairs for the transgenic human CEACAMs (5'–3'):
414 CEACAM3 (AACCCCAGGACAGCAGCTTC and GAGAGGCCTTTGTCCTGACC),
415 CEACAM5 (CATTTGCAACAGCTACAGTC and AGTGCAGTGGTATCAGAAAC)
416 CEACAM6 (TACTCAGCGTCAAAAGGAAC and AGAGACGTGGATCATCATCGTGA),
417 CEACAM7 (TGATCCTCCTGATTGTCACA CTACTGGGCAATACAACAGT). Mouse
418 interferon beta primers ATAAGCAGCTCCAGCTCCAA and
419 GCAACCACCACTCATTCTGA were used as positive control. Wild type littermates were
420 co-housed and used as controls. Mice were maintained under specific pathogen-free
421 conditions at the animal facility *Forschungszentrum Beutenberg, Zentrale Experimentelle*
422 *Tierhaltung*, University Hospital Jena, Germany, according to European and German animal
423 welfare regulations.

424 **4.3 Ethics statement**

425 Animal studies were performed in strict accordance with European (The Council of Europe's
426 European Convention, March 18, 1986, with the revised Annex A 2010/63/EU; The European
427 Parliament and Council Directive 2010/63/EU d 22.09.2010) and German animal welfare
428 regulations and the recommendations of the Society for Laboratory Animal Science (GV-
429 Solas). All experiments were approved by the ethics committee "Beratende Kommission nach
430 §15 Abs. 1 Tierschutzgesetz" and the responsible Federal State authority *Thüringer*
431 *Landesamt für Verbraucherschutz*, Bad Langensalza, Germany (Permit No. 02-019/14).

432 Studies with human materials were conducted according to the principles expressed in the
433 Declaration of Helsinki. Written informed consent to participate in this study or to allow the
434 use of residual material for research purposes was obtained. Protocols and use of cells for this
435 study were reviewed and approved by the institutional ethics committee of the Ethics
436 Committee of the Friedrich Schiller University Jena, Medical Faculty (permission numbers
437 5070-02/17 and 2020–1773).

438 **4.4 Systemic *C. albicans* infection model**

439 Systemic infection was performed as described previously[15]. Briefly, co-housed young adult
440 CEABAC10-transgenic mice (CEA) and their wild type littermates (WT) were injected with
441 2.5×10^4 CFU *C. albicans* /g body weight or 1×10^4 CFU *C. albicans*/g body weight via the
442 lateral tail vein. After the infection, mice were scored at least twice a day and sacrificed when
443 reaching a humane endpoint as described[15]. Log Rank comparison of the survival curves was
444 performed with the GraphPad PRISM 5 software.

445 For analyses at pre-defined time points after infection, mice were infected as described above
446 with 1×10^4 CFU *C. albicans* /g body weight ("Ca"). Control mice received endotoxin-free
447 buffered saline solution ("PBS", InVivoPure pH 6.5 Dilution Buffer, Hoelzel Diagnostika
448 GmbH, Germany; vehicle control). After infection, the health status of the mice was
449 examined as described[15], and mice were sacrificed after 24 h (PBS and Ca) or 72 h (Ca).
450 Since the vehicle control, PBS, does not result in any immune reaction[15], and any reaction due
451 to the stress of the application would be only short-lived, no additional PBS group was
452 analyzed at 72 h. Note that one PBS-injected CEABAC10 mouse was removed from all

453 analyses after histological analysis identified a high-grade hydronephrosis with associated,
454 presumably ascending pyelonephritis that was not associated with the experiment.

455 **4.5 Post mortem analyses**

456 When mice reached deep anesthesia, blood was taken retro-orbital and analyzed in an
457 automated hemocytometer (Mindray 5300Vet Hematology Analyzer). Peripheral blood for
458 the determination of cytokine levels and glycoproteome analysis (see below) was obtained via
459 cardiac puncture, kept at room temperature for 1 h and centrifuged at 1500 × g for 15 min
460 without break in order to obtain serum. Aliquots were kept at -80°C until further analysis.

461 During necropsy, kidneys, spleen, liver, and brain were removed, weighed and either fixed
462 immediately in Roti Histofix 4% (Carl Roth GmbH, Germany) and transferred into ethanol
463 the next day, or kept on ice in 1-3 ml PBS until homogenization. For pathohistological
464 analysis, a representative section from all organs was stained with hematoxylin and eosin and
465 evaluated histopathological. For visualization of fungal structures, a PAS reaction and Grocott
466 methenamine silver staining were performed. Histological preparations were digitalized with
467 an Aperio CS2 (Whole Slide Scanner, Leica), and size, area, and numbers of inflammatory
468 foci of the kidneys were quantified using the Image-Scope software (Leica). For development,
469 validation, evaluation, and statistical analysis, all embedded in the visual programming
470 language JIPipe[67] (https://jipipe.hki-jena.de/), where the automated image processing of
471 *Candida albicans* in mouse kidneys was realized using deep learning, please refer to
472 Supplemental Methods. DAB (3, 3'-diaminobenzidine) immunohistochemistry on paraffin
473 sections was performed after dewaxing (3 × xylol, 100% ethanol, 96% ethanol, 70% ethanol,
474 distilled water, 10 min, respectively), followed by citrate buffer, pH 6.0, at 96°C for 30 min.
475 After cooling, sections were washed with PBS and blocked with 1% BSA/PBS. Consecutive
476 sections were and incubated with 10 µg/ml 1H7-4B, anti-NE (neutrophil elastase) antibody
477 (Abcam, ab68672), and IgG control antibody (BioGenex, Rabbit NEGATIVE CONTROL)
478 respectively, followed by goat-anti-rabbit-Conjugate (Vector, VEC-BA-1000) and developed
479 using DAB (Carl Roth GmbH, Germany).

480 CFUs were determined by plating dilutions of organ homogenates on yeast extract-peptone-
481 dextrose (YPD) agar plates with 80 µg/ml chloramphenicol. The detection limits were as
482 follows: 50 CFU/g kidney and liver, respectively; 100 CFU/g spleen; 85 CFU/g brain. For
483 Multiplex analysis (Cytokine Mouse Magnetic 20-Plex Panel for the Luminex platform,
484 Thermo Fischer GmbH, Germany) or ELISA (mouse IL-6, IL-1β and TNF-A Ready Set Go,
485 both eBioscience, Germany; mouse IFNγ, BD Biosciences, Germany), homogenates were
486 centrifuged immediately at 3000 × g, 4°C for 10 min and aliquots of supernatants were kept at
487 -80°C until analysis.

488 For analysis of bone marrow cells, femurs were removed and kept in PBS on ice until cell
489 isolation procedures. The expression of human CEACAMs in bone marrow-derived
490 leukocytes fixed in 4% PFA/PBS was determined by flow cytometry. Cells were blocked in
491 500 µl of 10% BSA/PBS overnight at 4°C, treated with 1:30 mouse Fc block (eBioscience)
492 for 30 min at 4°C, and stained and analyzed as described in the respective (supplemental)
493 figure legends with the following antibodies and the corresponding isotype controls,
494 respectively: Ly6C PE-Cy 7, Ly6G-APC, huCD66acde-PE (all REA, Miltenyi Biotec), B220
495 PerCP-Cy 5.5, CD3-APC (both eBioscience). Samples were analyzed on an Attune Acoustic
496 Focusing Cytometer (Life Technologies, Thermo Fisher Scientific) using the FlowJo software
497 version 10.0.6.

498 The expression of human CEACAMs in viable immune cell populations isolated from kidney,
499 liver, and spleen was determined by flow cytometry. Cells were stained and analyzed on an
500 Attune Acoustic Focusing Cytometer (Life Technologies, Thermo Fisher Scientific) using the
501 Attune software v2.1 as described in the respective (supplemental) figure legends with the
502 following antibodies or the corresponding isotype controls: CD45-PE, Ly-6G-PerCP-Vio700,
503 CD3ε-PE-Vio770, CD19-APC, F4/80-FITC, CD45-PE, CD11c-PE-Vio770, CD335-APC (all
504 REA, Miltenyi Biotec), and viability dye eFluor780 (eBioscience).

505 **4.6 Glycoproteome analysis**

506 Glycoprotein enrichment from serum: After thawing, 20 µl serum were added to 20 µl 4%
507 SDS in PBS and heated for 5 min at 95°C. After cooling to room temperature, 60 µl of PBS
508 were added and the mixture was centrifuged at 20.000 x g for 10 min at RT. The supernatant
509 was used to enrich for glycoproteins as described[68]. Trypsin-released peptides and PNGase F-
510 released N-glycopeptides were collected and dried in a SpeedVac (ThermoScientific).
511 Shotgun MS-proteomics: Samples were reconstituted in 0.3% formic acid and peptide
512 concentrations were measured using a NanoDrop spectrometer. 2.5 µg of tryptic and of
513 deglycosylated peptides (former N-glycopeptides) were analyzed in each LC-MS/MS run in
514 duplicates on an Orbitrap Fusion (Thermo Scientific) coupled to a Dionex Ultimate 3000
515 (Thermo Scientific) by a nanoelectrospray ion source. Samples were loaded on a 2 cm C18
516 trap column (Acclaim PepMap100, Thermo Scientific) and separated using a 2.5 h non-linear
517 gradient (2-80% acetonitrile/0.1% formic acid, flow rate 300 nl/min) on a 50 cm C18
518 analytical column (75 µm i.d., PepMap RSLC, Thermo Scientific). Full MS scans were
519 acquired with resolution 120.000 at m/z 400 in the Orbitrap analyzer (m/z range 370-1570,
520 quadrupole isolation, isolation window 1.6). MS1 parent ions were fragmented by higher
521 energy collisional dissociation (HCD, 30% collision energy) and 20 fragment ion spectra were
522 acquired in the ion trap in rapid mode. The following conditions were used: spray voltage of
523 2.0 kV, heated capillary temperature of 275°C, S-lens RF level of 60%, maximum ion
524 accumulation times of 50 ms (AGC 1 x 106) for full scans and 35 ms (AGC 1 x 104) for
525 HCD. Protein Identification and Quantification: All RAW files were searched against the
526 human UniProt database (Version 05.2016, reviewed sequences) with MaxQuant version
527 1.5.5.1 (Max Planck Institute of Biochemistry[69]. The parameters were set as follows: main
528 search peptide tolerance: 4.5ppm; enzyme: trypsin, max. 2 missed cleavages; static
529 modification: cysteine carbamidomethylation; variable modification in the tryptic peptide
530 fraction: methionine oxidation; variable modification in PNGase F fractions: methionine
531 oxidation and asparagine deamidation. PSM (peptide specific matches) and protein FDR was
532 set to 0.01. For advanced identification the Second Peptide Search in MS2 spectra and the
533 Match Between Runs feature were enabled. Label-free quantification of proteins with
534 normalization was done in MaxQuant[69]. LFQ min. ratio count was set to one. Peptides from
535 both fractions were integrated in the LFQ protein intensity calculations. Only unique and
536 razor peptides, unmodified or modified, were used for quantification. LFQ protein intensities
537 (see Supplementary Table S7) were then loaded into the Perseus framework (Max Planck
538 Institute of Biochemistry)[70]. Known contaminants and reverse identified peptides/ proteins
539 were discarded. Intensities were log(2) transformed and missing values were imputed from
540 the normal distribution of the data set (width: 0.3, downshift 1.8). Two-sample T-test was
541 used to calculate statistical differences of protein abundances in the compared groups. P-
542 values were adjusted according to Benjamini and Hochberg[71], and proteins demonstrating at
543 least a two-fold expression difference and an adjusted p-value < 0.05 were considered to be
544 significantly changed in abundance. The mass spectrometry proteomics data have been
545 deposited to the ProteomeXchange Consortium via the PRIDE partner repository[72] with the
546 dataset identifier PXD061893 (reviewer account: Username: reviewer_pxd061893@ebi.ac.uk,
547 Password: ueEk3ftjm3Eq).

548 **4.7 Isolation and analysis of bone marrow-derived neutrophils (BMNs)**

549 Young adult mice were sacrificed by CO_2 inhalation. BMN were isolated and assessed for
550 purity and viability as described[15]. All assays were performed with freshly prepared BMN in
551 Eppendorf tubes blocked with 10% BSA/PBS, for at least 1 h at 37°C.

552 Concentration of released MPO was determined in cell culture supernatants from BMN that
553 were either left untreated or stimulated with live *C. albicans* yeast cells (MOI 10) for 60 min
554 using the mouse MPO ELISA kit (Hycultec GmbH).

555 *C. albicans* killing assay was performed using the Colorimetric Cell Viability Kits III (XTT)
556 from Promokine, Germany. 2×10^5 neutrophils in 100 µl RPMI/10% FBS were left
557 unstimulated or were stimulated with 2×10^5 *C. albicans* cells per well (MOI 1) in a 96 well
558 plate, for 30 min at 37°C, 5% CO_2. *C. albicans* solution for standards (input) was kept on ice
559 for the incubation times. Just before the following procedures, *C. albicans* standards
560 (sensitivity: 6,500 CFU) were transferred to the 96 well plate. Triton X-100 was added to all
561 wells to reach a final concentration of 0,3% and incubated for 10 min at 37°C, 5% CO_2, in
562 order inactivate neutrophils. Viable *C. albicans* cells were quantified by the addition of 50 µl
563 XTT reaction mixture per well and incubation for 3-4 h at 37°C, 5% CO_2. Absorbance was
564 measured using a TECAN M200 at 450 nm and 630 nm (background). For calculations of
565 *C. albicans* CFUs, background and blanks were subtracted.

566 Phagocytosis assays were performed as described[15]. Briefly, BMN were stimulated with
567 FITC-labeled *C. albicans* yeast cells (MOI 20) for 20 min, fixed and counterstained for
568 Hoechst33342 (Thermo Scientific), mouse anti-mouse CEACAM1 expressed on WT and
569 CEABAC10 BMN (MSCC1, monoclonal mouse IgG1, Bernhard B. Singer, Essen / highly
570 cross-adsorbed goat anti-mouse-Alexa546, Invitrogen) and extracellular *Candida* cells
571 (rabbit-anti Candida, BP1006, Acris antibodies / highly cross-adsorbed goat anti-rabbit-
572 Alexa633, Invitrogen). Micrographs were analyzed for phagocytosis by counting BMNs
573 without contact to *Candida* cells, BMN with attached, extracellular *Candida* cells (FITC
574 staining and anti-*Candida* antibody staining) and BMN with intracellular (phagocytosed)
575 *Candida* cells (FITC staining only) with a confocal laser scanning microscope (Zeiss LSM
576 710) using the ZEN 2010 software (both Carl Zeiss Microscopy GmbH).

577 All flow cytometric analyses of BMN were performed on an Attune Acoustic Focusing
578 Cytometer (Life Technologies, Thermo Fisher Scientific) using the Attune software v2.1.

579 The expression of CD11b, and human CEACAM3 and CEACAM6 and their relative
580 fluorescence intensities on BMN was determined in cells either left untreated or stimulated
581 with UV-killed *C. albicans* germ tubes (MOI 10) for 60 min. Cells were stained using
582 viability dye eFluor780 (eBiosciences), anti-CD11b-APC (clone REA592, Miltenyi Biotec),
583 and either 308/3-3 (anti-human CEACAM3/5, LeukoCom, Essen, Germany) / highly cross-
584 adsorbed goat anti-mouse IgG1-PE (eBiosciences), or 1H7-4B (anti-human CEACAM6,
585 LeukoCom, Essen, Germany) / highly cross-adsorbed goat anti-mouse IgG1-PE
586 (eBiosciences), respectively. Note that 308/3-3 cross-reacts to CEACAM5[14] that is not
587 expressed on neutrophils (therefore we refer to 308/3-3 as "CEACAM3-specific" in the
588 context of this publication). For the analysis of flow cytometry data, dead cells were excluded
589 due to possible false positive staining.

590 For analysis of apoptosis, BMN were either left untreated for 2 h, or were treated for 2 h with
591 UV-killed *C. albicans* germ tubes (MOI 10) and stained using the Annexin V Detection Kit

592 APC (eBiosciences). Cells negative for Annexin V and propidium iodide were considered
593 viable.

594 Analysis of intracellular reactive oxygen species was performed as described[15]. Briefly, BMN
595 were pre-incubated for 15 min with 1.5 µg/ml dihydro-rhodamine 123 (DHR, Biomol GmbH)
596 in calcium- and magnesium-free PBS/2.5% BSA and either left untreated or stimulated with
597 UV-killed *C. albicans* germ tubes (MOI 10) for another 15 min. Cells were washed in
598 calcium- and magnesium-free PBS, fixed in 1% PFA/PBS for 10 min, blocked with PBS/50%
599 heat-inactivated fetal bovine serum, and washed with PBS/2% heat-inactivated fetal bovine
600 serum.

601 **4.8 Differentiation and analysis of bone marrow-derived monocytes (BMM) and**
602 **macrophages (BMDM)**

603 Young adult mice were sacrificed by CO_2 inhalation. Isolated bone marrow cells were
604 differentiated into BMM (non-adherent cells, 5-7 days) and BMDM (adherent cells, 7 days) in
605 RPMI/25 ng/ml recombinant mouse M-CSF (ImmunoTools GmbH, Friesoythe, Germany).
606 The medium was exchanged every other day (non-adherent cells were collected by
607 centrifugation). CEACAM6 expression was determined by flow cytometry using eFluor 780
608 (eBioscience, USA), and the following antibodies (all Miltenyi Biotec): CD66c-PE / REA414
609 (CEACAM6), F4/80-FITC / REA126, CD11b-APC / REA892, CD11c-PE-Vio770/REA754,
610 CD62L-APC / REA828 as described in the respective (supplemental) figure legends. All flow
611 cytometric analyses of BMN and BMDM, respectively, were performed on an Attune
612 Acoustic Focusing Cytometer (Life Technologies, Thermo Fisher Scientific) using the Attune
613 software v2.1.

614 For stimulation, *C. albicans* was opsonized (2×10^8 / 1 ml of serum, incubation on ice for at
615 least one hour, removal of serum by RPMI wash). In all stimulations longer than 6 h,
616 treatment of the cells with Amphotericin B was included to prevent excessive growth of
617 hyphae (1 µg/ml, added after 1 h of stimulation). For the phagocytosis assay, *C. albicans* cells
618 were labelled with fluorescein isothiocyanate (FITC) prior to the experiment (see above).

619 For ELISAs, 5×10^5 BMN and BMDM, respectively, in 500 µl medium were seeded in 24-
620 well-plates, and were either left untreated, or were stimulated for 24 h at MOI 1.
621 Concentrations of mouse cytokines IL-1β (eBioscience), IL-6 (Thermo Scientific), CCL2
622 (Becton Dickinson), and TNFα (Thermo Scientific) were determined according to
623 manufacturer's instructions.

624 To quantify the overall *C. albicans*-induced cell death, BMDM were seeded in 48-well-plates
625 at a density of 2.5×10^5 cells in 250 µl of medium. Following 24 h of *C. albicans* stimulation
626 at MOI 1, SYTOX^{TM} Green (Invitrogen, USA) was added to the cells to a final concentration
627 of 200 nM and incubated for 10 min in the dark at 37 °C 5 % CO_2. Two images per well were
628 taken at 20x magnification using the Vert.A1 + AxioCam MRc (Carl Zeiss, Germany) and
629 exported as .tiff files from ZEN software (Carl Zeiss, Germany). Cells were counted using the
630 multi-point tool in Image J (open source). Phase-contrast images were used to count all cells
631 and dead cells were counted in the SYTOX^{TM} Green channel.

632 For analysis of phagocytosis, 2.5×10^5 BMDM/well were seeded in collagen-coated 8-well-
633 chambers (Permanox, Nunc Lab-TEK, Thermo Scientific) in 500 µl of medium and
634 stimulated at an MOI 5 with FITC-labeled *C. albicans* for 20 min. Cells were washed twice
635 with pre-warmed PBS, fixed with 250 µl 4% paraformaldehyde in PBS for 20 min at RT, and
636 blocked with 200 µl 10 % BSA/PBS at 4°C overnight. Mouse Fc-block (eBioscience) was

637 added for 30 min, and rabbit-anti-*Candida* antibody (BP1006, Acris antibodies) was added at
638 5 µg/ml for 1 h. Cells were washed three times with PBS, and goat anti-rabbit-Alexa Fluor
639 633 antibody (1:200, Invitrogen) and Hoechst33342 (1:1000, Thermo Scientific) in 5%
640 BSA/PBS were added. Cells were washed three times with PBS, chambers were removed, and
641 the slides were dipped consecutively in PBS, water and 70 % ethanol. After drying, slides
642 were mounted with Vectashield mounting medium and allowed to harden in the dark
643 overnight at RT and sealed using nail polish. Samples were analyzed with a Cell Observer Z1
644 microscope (Carl Zeiss, Germany) using the ZEN2010 software. Intracellular Ca and BMDM-
645 associated extracellular Ca were counted, and the number of extracellular Ca was divided by
646 the number of intracellular plus associated Ca, giving the phagocytosis index.

647 **4.9 Human liver section analysis**

648 Human PFA-fixed, paraffin-embedded liver sections were incubated at room temperature
649 consecutively with xylol (2x 15 min), 100% ethanol, 96% ethanol, 70% ethanol, and with
650 distilled water (each for 10 min), followed by Tris-EDTA buffer, pH 9.0, at boiling
651 temperature for 15 min. After cooling, sections were washed with PBS and blocked with 1%
652 BSA/PBS, incubated with monoclonal rabbit-anti-CD68 antibody (EPR20545, Abcam) and
653 mouse anti-CEACAM6 1H7-4B, (LeukoCom, Essen, Germany) at 10 µg/ml in 0.5% BSA
654 over night at 4°C in a humid chamber, washed and incubated with "Goat anti-Rabbit IgG
655 (H+L) Cross-Adsorbed Secondary Antibody -Alexa Fluor 660" (Thermo Scientific), "Alexa
656 Flour 546 Goat anti Mouse IgG (H+L)" (Invitrogen GmbH), each 1:200 in 0.5% BSA, and
657 1:5000 Hoechst 33342" (Thermo Scientific) for 1h at RT. Slides were washed twice with
658 PBS. After drying, slides were mounted with Vectashield mounting medium (Biozol),
659 allowed to harden in the dark overnight at RT, and sealed using nail polish. Samples were
660 analyzed with an Axio Observer.Z1/7 microscope using the ZEN 2010 software (both Carl
661 Zeiss Microscopy GmbH).

662 **4.10 Human alveolar macrophage analysis**

663 Cells from human bronchoalveolar lavage were stained for CD169-PE (marker for alveolar
664 macrophages), CD66b-FITC (marker for human neutrophils), and CEACAM6 (CD66c-PE-
665 Vio770) (all REA, Miltenyi Biotec) and analyzed on an Attune Acoustic Focusing Cytometer
666 (Life Technologies, Thermo Fisher Scientific) using the Attune software v2.1.

667 **4.11 Human peripheral monocyte analysis**

668 Human PBMCs were isolated and stained directly using anti-CD14-FITC (REA, Miltenyi
669 Biotec), anti-CD66c.PE-Vio770 (CEACAM6, REA, Miltenyi Biotec, and eFluor780. Cells
670 were analyzed on an on an Attune Acoustic Focusing Cytometer (Life Technologies, Thermo
671 Fisher Scientific) using the Attune software v2.1.

672 **4.12 Statistical analysis**

673 Except for proteomics data, statistical analysis was performed using GraphPad Prism 5.04
674 Software. For parametric data with 2 groups, unpaired, two-tailed Students t-test was
675 performed; for matched pairs, a paired two-tailed Students t-test was performed. For non-
676 matched parametric data with more than 2 groups, one-way ANOVA with Bonferroni post-
677 tests was performed. In case of exponential data (CFUs, relative fluorescence intensity)
678 log(10) transformed data were used for statistical analysis. In case of samples with no
679 detectable CFU counts, statistical analysis was performed twice, inserting either 0.1 or the
680 respective detection limit; the outcome was “not significant” in both cases. In the present
681 manuscript, p values for the former analysis are given.

5 Data Availability

The datasets generated during and/or analyzed during the current study are available in the ProteomeXchange Consortium via the PRIDE partner repository72 with the dataset identifier PXD061893 (reviewer account: Username: reviewer_pxd061893@ebi.ac.uk, Password: ueEk3ftjm3Eq). Code used for image analysis (see supplemental Material / supplemental method) is available at: https://asbdata.hki-jena.de/Klaile_PraetoriusEtAl2023_NatCommun

6 Acknowledgment

We thank Simone Tänzer, Moira Stark, Birgit Weber and Katja Schubert for their excellent technical assistance. We sincerely thank Bernhard B. Singer (†2024), a close colleague, friend, and leading expert in the field. His constant support, expertise, and groundbreaking design of CEACAM-specific antibodies were instrumental in raising the quality of CEACAM research to a level that would not have been possible without him. His visionary contributions significantly advanced CEACAM research worldwide.

7 Author Contributions

EK and HS conceived the study. EK, MMM, JS, AKB, SB, JE, TEK, SK and IDJ performed experiments. EK, MMM, JS, AKB, SB, JE, SK, AG, KD, OK, JPP, and MTF analyzed data. EK drafted the manuscript. EK, MMM, JS, AKB, SB, JE, TEK, SK, KD, OK, JPP, MTF, TB, AG, GM, IDJ and HS revised and approved the manuscript.

8 Funding

This work was supported by the German Research Foundation via the Collaborative Research Center/Transregio 124—Pathogenic fungi and their human host: Networks of Interaction (project number 210879364, Project A5 to HS, Project C5 to IDJ and Project B4 to MTF). This work was supported by „Stiftung Oskar Helene Heim“. SB and JE were IZKF-Fellows (doctoral scholarships of the Interdisziplinäres Zentrum für Klinische Forschung, Jena, Germany). The funders had no role in study design, data collection and analysis, decision to publish, or preparation of the manuscript.

9 Conflict of Interest Statement

The authors declare that the research was conducted in the absence of any commercial or financial relationships that could be construed as a potential conflict of interest.

10 Contribution to the Field Statement

Systemic *C. albicans* infections result in an extremely high morbidity and mortality and still pose a major challenge regarding early diagnosis and treatment. Three myeloid cell types are first responding to systemic microbial infections: neutrophils, monocytes, and macrophages. The CEABAC10 transgenic mice express *Candida* receptors of the human CEACAM receptor family on their innate immune cells and on their mucosa. In the present study we show for the first time that the expression of human CEACAM6 on monocytes and macrophages can be essential to the regulation of the host response to pathogens. So far, only the expression of different CEACAM receptors on neutrophils and in mucosal epithelial cells was described to regulate the innate immune response to microbial infection. This work therefore points toward a completely new direction regarding the CEACAM-dependent regulation of immune responses.

723 **11 Figures and Figure Legends**

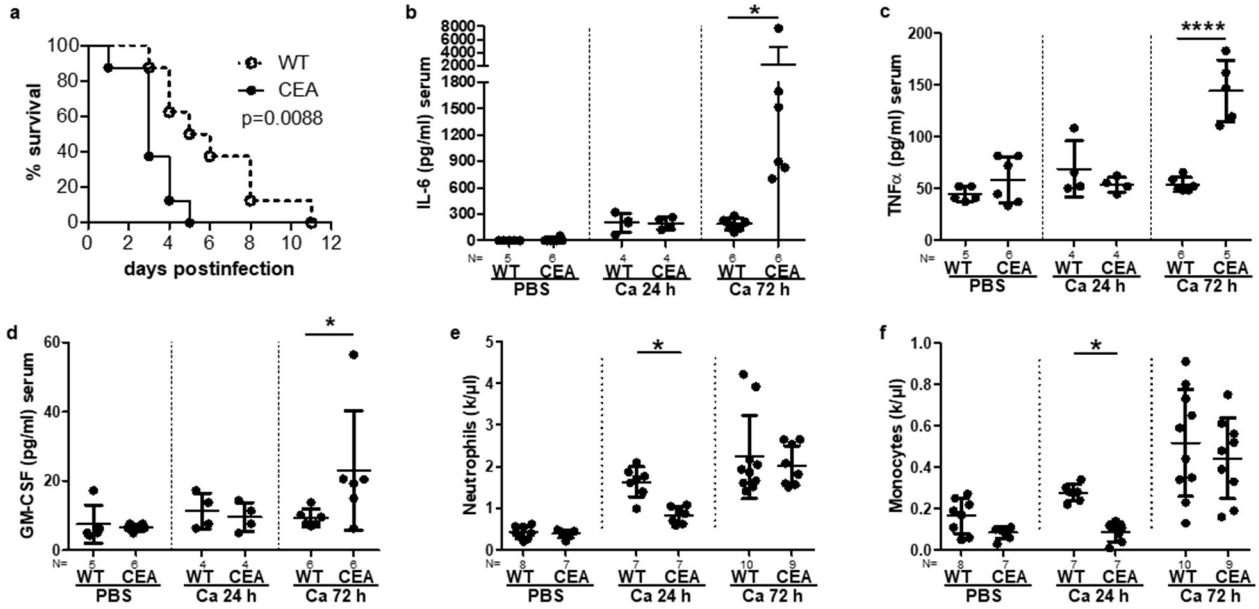

724

725 **Figure 1: CEABAC10 mice are more susceptible to systemic *C. albicans* infection.** (a)
726 CEABAC10 mice (N=8) and wild type littermates (N=8) were injected with 1×10^4 CFU
727 *C. albicans* /g body weight and were analyzed for survival (one experiment). Note that
728 significant results were also obtained after injection of 2.5×10^4 CFU/g body weight (Figure
729 S1). (b-f) CEABAC10 mice and wild type littermates were either injected with PBS or
730 infected with 1×10^4 CFU/g body weight, respectively, and were sacrificed after 24 h or 72 h.
731 Cytokine levels in peripheral blood were determined for IL-6 (b), TNFα (c) and GM-CSF (d)
732 by multiplex assay (Luminex) or ELISA. Additional cytokines are shown in Figure S2.
733 Numbers of neutrophils (e) and monocytes (f) in peripheral blood were analyzed in an
734 automated hemocytometer (additional blood parameters in Figure S4). Statistics: (a) Log rank
735 test (Mantel Cox); (b-f) One-Way-ANOVA and Bonferronis' Multiple Comparison Test:
736 *p<0.05 ****p<0.001. Data are from one experiment (a) or combined from two independent
737 experiments (b-f). (b-f) Data points with mean and standard deviation.

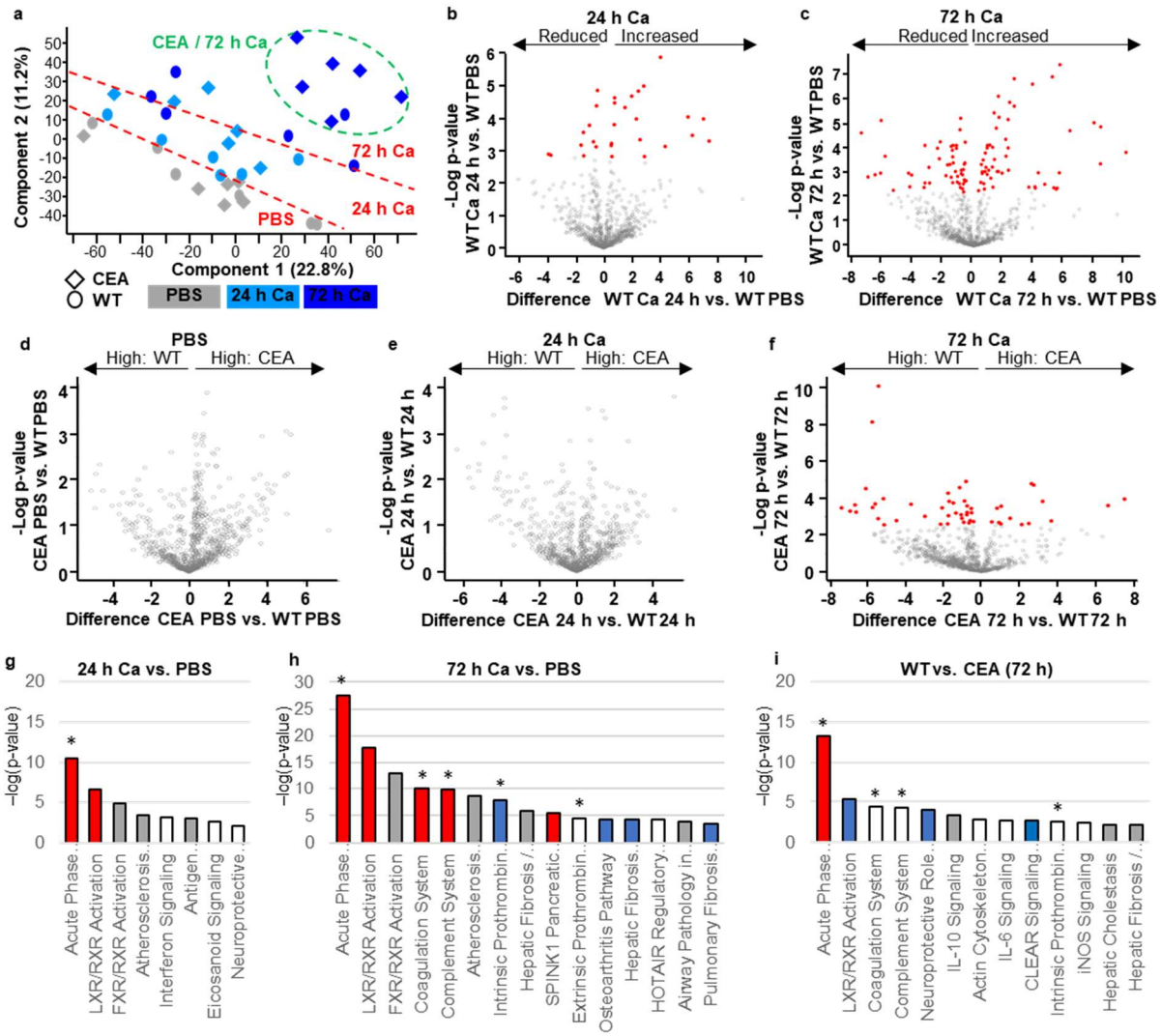

Figure 2: Enhanced acute phase response in CEABAC10 mice after 72 h systemic *C. albicans* infection. CEABAC10 mice and wild type littermates were either injected with PBS or infected with 1×10^4 CFU/g body weight, respectively, and were sacrificed after 24 h or 72 h (N=6 per group, combined from two independent experiments). Glycoproteins were isolated from serum and analyzed via mass spectrometry. (a) Principal component analysis of identified proteins. Note that PBS injected mice and mice 24 h p.i. and 72 h p.i. separate, respectively, (dashed red lines) but that CEABAC10 samples only separate from WT samples 72 h p.i. (dashed green oval). (b, c) Volcano plots of contrasts of WT samples 24 h p.i. (b) and 72 h p.i. (c) vs. WT PBS, respectively. Plots display –log(p-value) versus the mean difference (log(2) fold-change). Red dots indicate statistically significant changes. All proteins detected and their corresponding values are listed in Tables S1 (b) and S2 (c). (d-f) Volcano plots of contrasts of CEABAC10 vs. WT samples from PBS controls (d), 24 h p.i. (e), or 72 h p.i. (f). Plots display –log(p-value) versus the mean difference (log(2) fold-change). Red dots indicate statistically significant changes. All proteins detected and their corresponding values (f) are given in Table S4. Note that in (d) and (e) no significant alterations were observed. (g-i) Pathway analysis of fold-changes in glycoprotein levels found in (b), (c), and (f), respectively. Asterisks (*) mark extracellular pathways. Bars are color coded for z-scores: red = positive z-score (activated); blue = negative z-score (inhibited); white = z-score equals 0; grey: no activity pattern available. Statistical analysis: MaxQuant, Perseus, and IPA software (settings: materials and methods section).

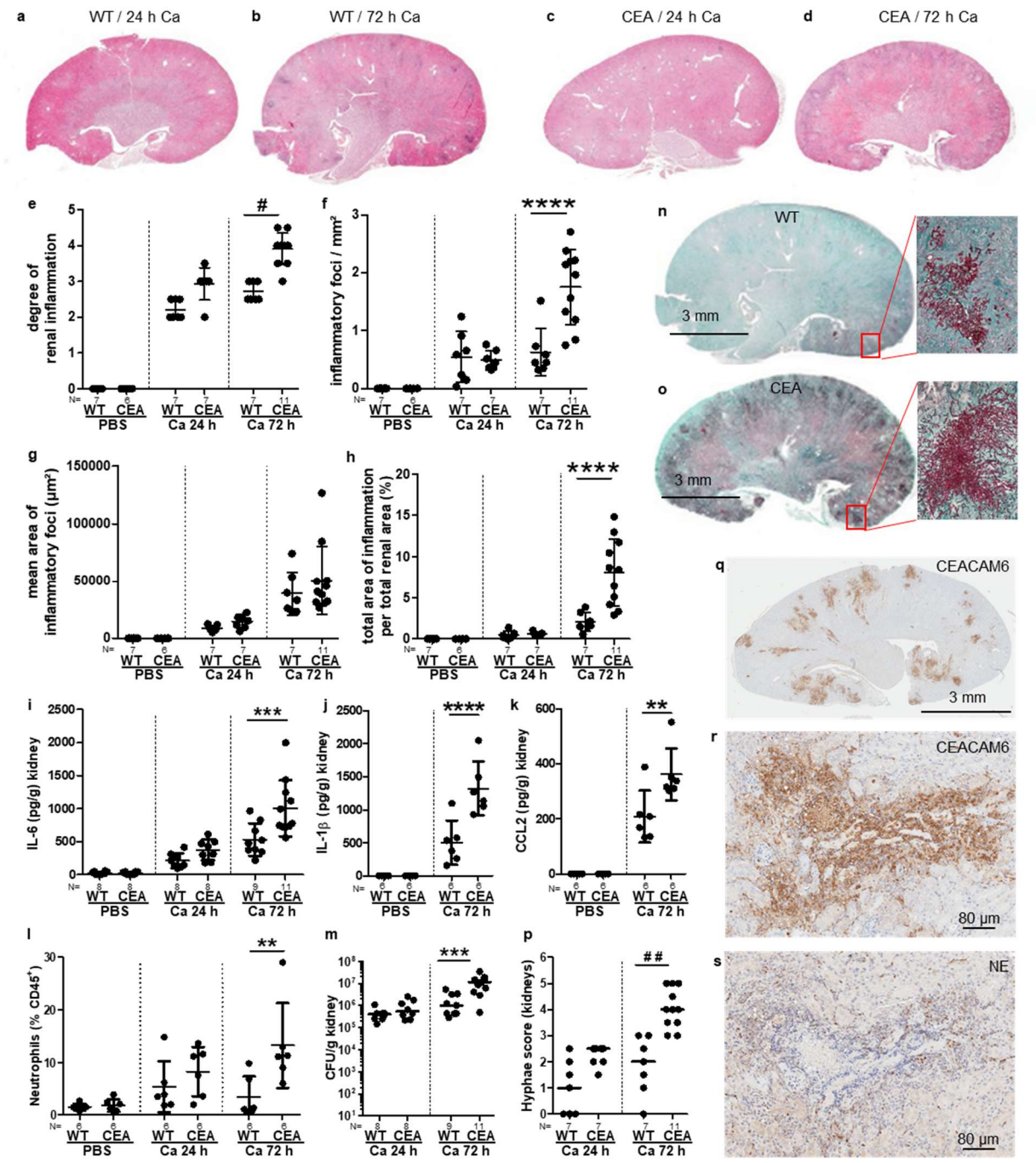

759

760 **Figure 3: CEABAC10 mice show enhanced kidney inflammation during systemic**
761 ***C. albicans* infection.** CEABAC10 mice and wild type littermates were either injected with
762 PBS or infected with 1×10^4 CFU/g body weight, respectively, and were sacrificed after 24 h
763 or 72 h. (a-h) Kidney sections were hematoxylin-eosin-stained and analyzed. (a-d)
764 Representative sections of WT and CEABAC10 kidneys. Sections were scored for the degree
765 of renal inflammation (e) and analyzed for inflammatory foci (f, g) and total area of
766 inflammation (h). (i-k, m) Concentrations of IL-6 (i), IL-1β (j) and CCL2/MCP-1 (k), and
767 CFUs (m) were determined in kidney homogenates by multiplex assay (Luminex)/ELISA and
768 serial plating, respectively (additional cytokines in Figure S5). (l) % $Ly6G^+$ neutrophils of
769 $CD45^+$ leukocytes isolated from kidneys analyzed by flow cytometry (additional immune cell
770 populations in Figure S6, gating in Figure S7). (n, o) Representative Grocott-silver-stained
771 sections 72 h p.i and blow-ups of the indicated regions. (p) Grocott-silver-stained sections
772 were scored for the occurrence of hyphal growth. Note that non-infected kidneys (8 WT and 8

CEABAC10 / PBS) did not show fungal growth (l, o). (q-s) Immunohistochemical staining of consecutive sections of CEABAC10 kidneys 72 h p.i for CEACAM6 (q, r) or neutrophil elastase (s), respectively. Panels display representative images (N=3). Note that only viable neutrophils are NE$^+$, but that CEACAM6$^+$ cells include viable and dead neutrophils, monocytes, and macrophages, and that CEACAM6$^+$ cells (r) outnumber viable neutrophils (s) by ca. one or two orders of magnitude. Statistics: (e, o) Kruskal-Wallis and Dunn's Multiple Comparison Test, #p<0.05, ##p<0.01; (f-l, p) One-Way-ANOVA and Bonferronis' Multiple Comparison Test: *p<0.05 **p<0.01 ***p<0.005 ****p<0.001. (e-k) Data points with mean and standard deviation. (m, p) Data points with median and mean, respectively. Data are combined from two independent experiments.

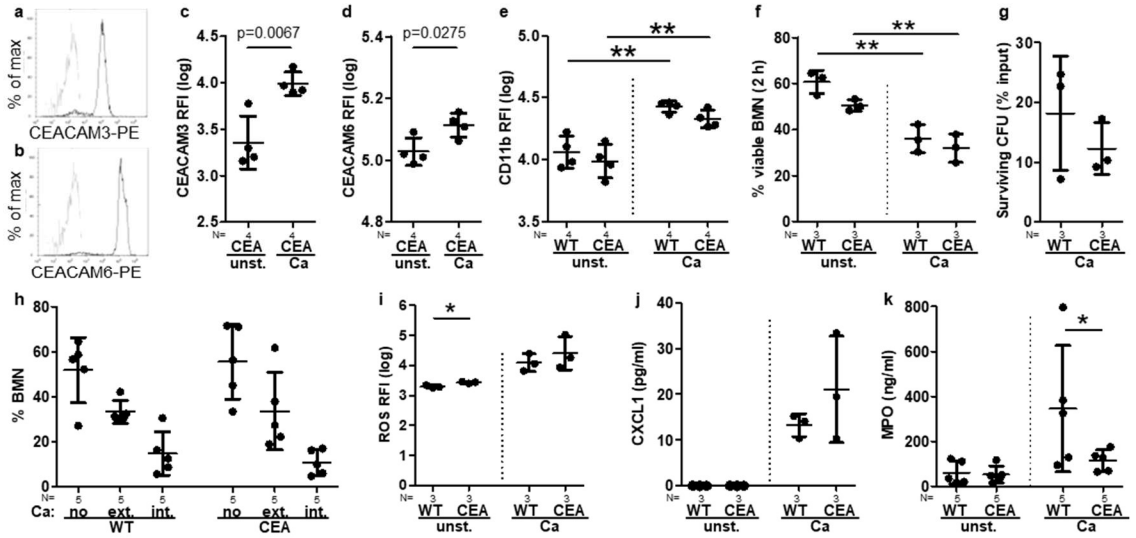

Figure 4: WT and CEABAC10 bone marrow-derived neutrophils display similar reactions to *C. albicans*. (a-e) Degranulation and CEACAM surface expression. WT and CEABAC10 BMN were either left untreated or stimulated with *C. albicans* for 1 h, stained for CD11b and either CEACAM3 (a, c), or CEACAM6 (b, d), respectively, and analyzed by flow cytometry (gating in Figure S8). (a, b) Representative results, grey line: isotype control, black lines: CEACAM3 and CEACAM6, respectively. (c-e) Log data of the relative fluorescence intensity (RFI) with mean and SD. (f) Spontaneous and *C. albicans*-induced cell death after 2 h. Viability was assessed by exclusion of PI and annexin V staining via flow cytometry (% viable BMN with mean and SD). (g) *C. albicans* killing efficiency after 30 min analyzed by XTT assay (% surviving CFUs from the input with mean and SD). (h) *C. albicans* binding/phagocytosis (20 min, FITC-labeled yeast cells at MOI 10, stained for extracellular *C. albicans* via specific antibody) was analyzed by fluorescence microscopy for cells with no contact to *C. albicans* (no), with *C. albicans* bound exclusively extracellular (ext.), and phagocytosed, intracellular *C. albicans* (int.) (% BMN with mean and SD). For each experiment, at least 100 BMN were counted per group. (i) Spontaneous and *C. albicans* -induced production of reactive oxygen species (ROS) after 20 min measured via DHR assay by flow cytometry (log data of RFI with mean and SD. (k, l) Spontaneous and *C. albicans*-induced CXCL1/KC (k) and myeloperoxidase (MPO) (l) release in cell culture supernatants after 24 h with mean and SD. Statistics: (c, d, g) unpaired, two-sided Student's T test; (e, f, h, i, j, k) One-Way-ANOVA and Bonferronis' Multiple Comparison Test: *p<0.05 **p<0.01; log data were used for statistical analysis of (c-e, i). (c-k) Data points with mean and standard deviation.

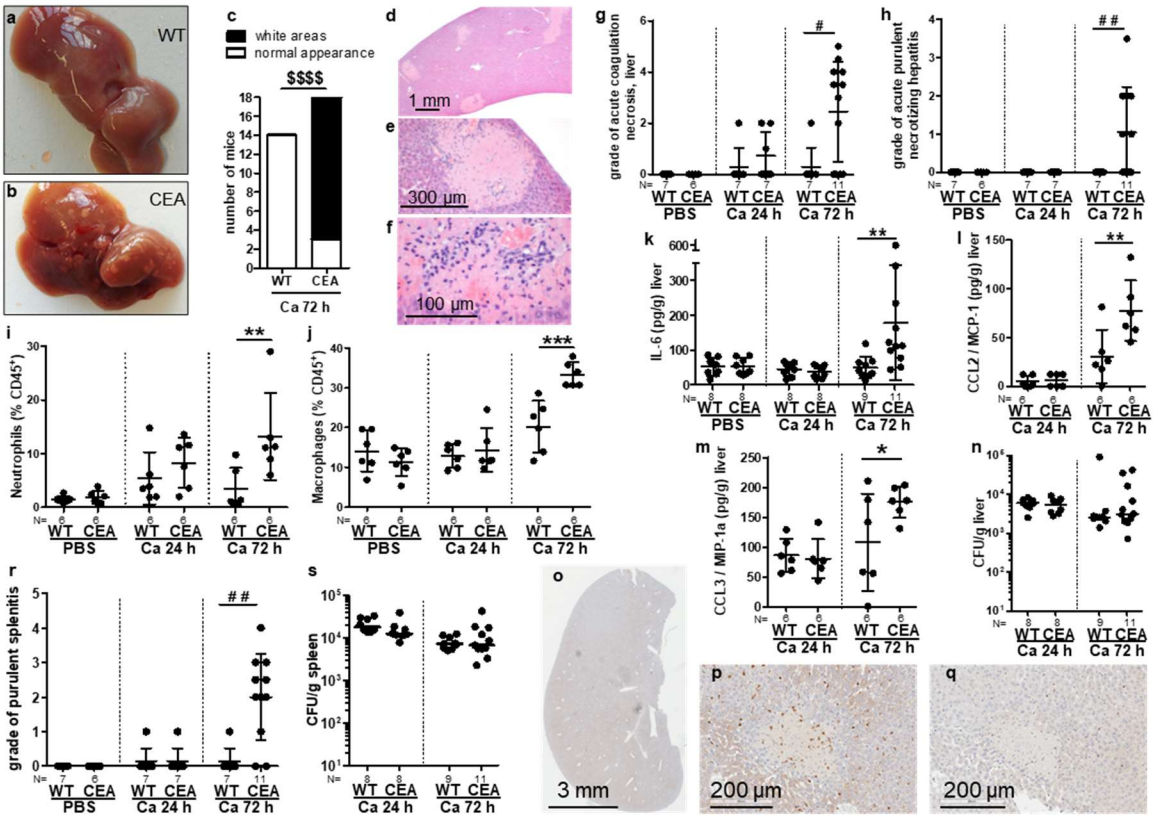

Figure 5: CEABAC10 livers display enhanced inflammation, acute coagulation necroses with immune cell infiltration, and multifocal hemorrhage during systemic *C. albicans* infection. CEABAC10 mice and wild type littermates were either injected with PBS or infected with 1×10^4 CFU/g body weight, respectively, and were sacrificed after 24 h or 72 h. (a-c) Occurrence of macroscopic pathologic liver abnormalities (white areas) observed during necropsy 72 h p.i. (18 CEA, 14 WT). (a, b) Representative images. (c) Livers without macroscopic abnormalities (open bars), and livers displaying white areas 72 h p.i. (filled bars). (d-h) Liver sections were hematoxylin-eosin-stained and analyzed. (d-f) Representative CEABAC10 liver section 72 h p.i., showing acute coagulation necroses with immune cell infiltration and multifocal hemorrhage. (g, h) Sections were scored for the degree of acute coagulation necroses (g) and for the grade of acute purulent necrotizing hepatitis (h). (i, j) % $Ly6G^+$ neutrophils (i), and $F4/80^+$ macrophages (j) of $CD45^+$ leukocytes isolated from livers (additional immune cell populations in Figure S10, gating in Figure S11). (k-m) Concentrations of IL-6 (k), CCL2/MCP-1 (l) and CCL3/MIP-1alpha (m) were determined in liver homogenates (additional cytokines in Figure S9). (n) CFUs in liver homogenates. (o-q) Immunohistochemical staining of consecutive CEABAC10 liver sections 72 h p.i. for CEACAM6 (o, p) or neutrophil elastase (NE) (q), respectively (representative sections, N=3). Note that only viable neutrophils are NE^+, but that $CEACAM6^+$ cells include viable and dead neutrophils and macrophages/monocytes, and that $CEACAM6^+$ cells (p) outnumber viable neutrophils (q) by one or two orders of magnitude. (r) Spleen sections were hematoxylin-eosin-stained and scored for splenitis. (s) CFUs were determined in spleen homogenates. Note that livers and spleens from uninfected animals (8 WT and 8 CEABAC10 for PBS, respectively) did not display any fungal growth and that none of the infected liver and spleen samples displayed any hyphal growth. Data are combined from two (g-n, r, s) or four (c) independent experiments. Statistics: (c) Fisher's Exact Test, two-sided $$$$ $p<0.001$; (g, h, r) Kruskal-Wallis and Dunn's Multiple Comparison Test, #$p<0.05$ ##$p<0.01$; (i-n, s) One-Way-ANOVA and Bonferronis' Multiple Comparison Test: *$p<0.05$ **$p<0.01$. For (l, s), log data were used for statistical analysis. (g-n, r, s) Data points with mean and standard deviation.

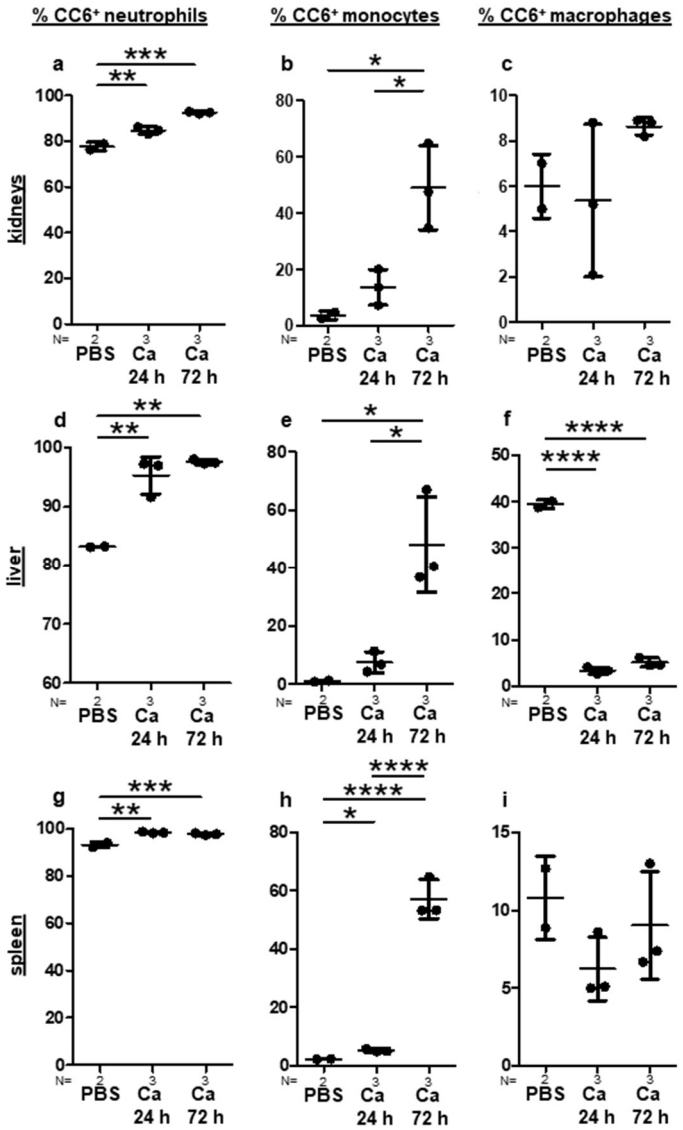

Figure 6: Increased numbers of CEACAM6+ myeloid cells in organs of CEABAC10 mice during systemic *C. albicans* infection, and loss of CEACAM6+ liver macrophages. CEABAC10 mice were either injected with PBS or infected with 1×10^4 CFU/g body weight, respectively, and were sacrificed after 24 h or 72 h. Immune cells were isolated from kidneys, liver, and spleen, and stained for viability dye/CD45/CD11b/Ly6G, and viability dye/CD45/F4/80/Ly6C/CD11c, respectively. Neutrophils, monocytes, and macrophages were analyzed for their percentage of human CEACAM6-positive cells (gating: see Figure S15). Graphs give the percentage of CEACAM6-positive cells of the respective cell type with mean and standard deviation. Data are from one experiment. Statistics: One-Way-ANOVA and Bonferronis' Multiple Comparison Test: *p<0.05 **p<0.01 ***p<0.005 ****p<0.001.

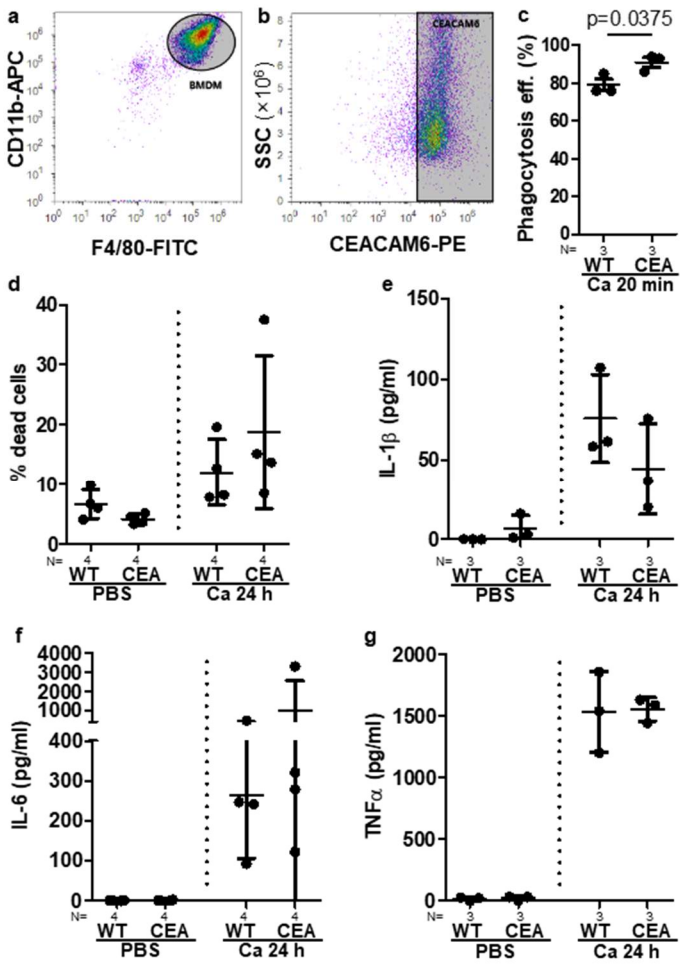

Figure 7: Enhanced phagocytosis but unaltered *C. albicans*-induced cell death of CEACAM6$^+$ bone marrow-derived macrophages. (a, b) Bone marrow-derived macrophages (BMDM) from CEABAC10 mice were analyzed via flow cytometry. Single viable cells were gated for F4/80$^+$/CD11b$^+$ macrophages (a) and analyzed for their CEACAM6 expression (b); for complete gating see Figure S16. Graphs are representative of three independent experiments (mean and standard deviation: 88.9%±5.1%CEACAM6$^+$ BMDM). (c) WT and CEABAC10 BMDM were incubated with FITC-labeled *C. albicans* at MOI 5 for 20 min, fixed, and stained for extracellular *C. albicans*. Images were analyzed for *C. albicans* bound externally to BMDM, and phagocytosed/intracellular *C. albicans*. The graph gives the phagocytosis efficiency in %: intracellular *C. albicans* / (externally bound + intracellular *C. albicans*) × 100. N=3, at least 100 cells were analyzed per sample. (d) WT and CEABAC10 BMDM were either left unstimulated or incubated with *C. albicans* at MOI 1 for 24 h and analyzed for the percentage of dead cells by Sytox green staining; at least 100 cells were analyzed per sample. (e-g) WT and CEABAC10 BMDM were either left unstimulated or incubated with *C. albicans* at MOI 1 for 24 h. Concentrations of IL-1β (e), IL-6 (f), and TNFα (g), were determined in cell culture supernatants via ELISA. Graphs give data points with mean and SD. Statistics: (c) unpaired two-sided Student's T test; (d-g) One-Way-ANOVA and Bonferronis' Multiple Comparison Test. (c-g) Data points with mean and standard deviation.

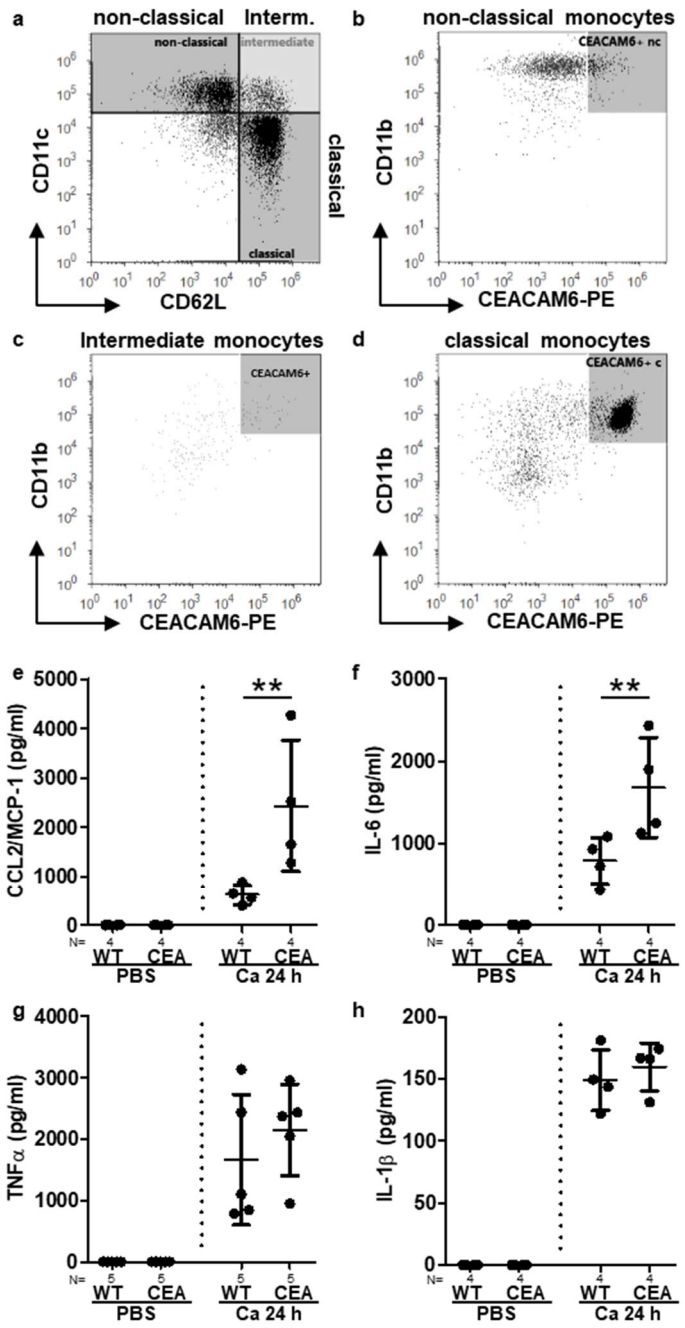

Figure 8: Bone marrow-derived CEACAM6$^+$ classical monocytes release enhanced amounts of IL-6 and CCL2 in response to *C. albicans* infection. (a-d) Bone marrow-derived monocytes (BMM) from CEABAC10 mice were analyzed by flow cytometry. Single viable BMM were gated into CD11c$^+$/CD62L$^-$ non-classical monocytes, CD11c$^+$/CD62L$^+$ intermediate monocytes, and CD11c$^-$/CD62L$^+$ classical monocytes (a), and analyzed for their CEACAM6 and CD11b expression (b-d, respectively). For complete gating see Figure S16. Graphs are representative of three independent experiments (mean and standard deviation: CEACAM6$^+$ non-classical monocytes = 1,6%±0.4%; CEACAM6$^+$ intermediate monocytes = 36.9%±3.8%; CEACAM6$^+$ classical monocytes = 83.4%±6.4%). (e-h) WT and CEABAC10 BMM were either left unstimulated or incubated with *C. albicans* at MOI 1 for 24 h. Concentrations of CCL2/MCP-1 (e), IL-6 (f), TNFα (g), and IL-1β (h), were determined in cell culture supernatants. Graphs give data points with mean and standard deviation. Statistics: One-Way-ANOVA and Bonferronis' Multiple Comparison Test, **$p<0.01$.

883 **12 Supplementary Material**

884 Supplementary Figures and Method (PDF file):

885 Figure S1: CEABAC10 mice are more susceptible to systemic *C. albicans* infection. Survival
886 analysis with an infection dose of 2.5×10^4 CFU/g body weight. Related to Figure 1.

887 Figure S2: CEABAC10 mice display enhanced cytokine levels in peripheral blood during
888 systemic *C. albicans* infection. Multiplex/ELISA. Related to Figure 1.

889 Figure S3: No differences in bone marrow compositions between WT and CEABAC10 mice
890 during systemic *C. albicans* infection. Flow cytometry.

891 Figure S4: CEABAC10 mice have reduced white blood cell and platelets in counts in their
892 peripheral blood during systemic *C. albicans* infection. Automated cytometric analysis of
893 peripheral blood. Related to Figure 1.

894 Figure S5: CEABAC10 mice have enhanced cytokine concentrations in their kidneys during
895 systemic *C. albicans* infection. Multiplex/ELISA. Related to Figure 3.

896 Figure S6: Immune cell populations in kidneys of WT and CEABAC10 mice during systemic
897 *C. albicans* infection and automated image analysis of *Candida* cells kidney sections. Related
898 to Figure 3.

899 Figure S7: Gating of immune cell populations in kidneys. Related to Figure 3 and Figure S6.

900 Figure S8: BMN gating. Related to Figure 4.

901 Figure S9: CEABAC10 mice have enhanced CCL3 and CXCL10 concentrations in their
902 livers during systemic *C. albicans* infection. Multiplex/ELISA. Related to Figure 5.

903 Figure S10: Immune cell populations in livers of WT and CEABAC10 mice during systemic
904 *C. albicans* infection. Flow cytometry and IHC. Related to Figure 5.

905 Figure S11: Gating of immune cell populations in livers. Related to Figure 5 and Figure S10.

906 Figure S12: Immune cell populations in spleen during systemic *C. albicans* infection. Flow
907 cytometry and IHC. Related to Figure 5.

908 Figure S13: Gating of immune cell populations in spleens. Related to Figure S12.

909 Figure S14: CEABAC10 mice display brain hemorrhage but no increase in encephalitis 72 h
910 post-*C. albicans* infection. Fungal load, histopathologic analysis, IHC.

911 Figure S15: Gating of CEACAM6$^+$ myeloid cells in organs of CEABAC10 mice during
912 systemic *C. albicans* infection. Related to Figure 6

913 Figure S16: Gating of bone marrow-derived macrophages and monocytes. Related to Figures
914 7 and 8.

915 Figure S17: CEACAM6 expression on human liver macrophages.

916 Figure S18: CEACAM6 expression on human alveolar macrophages.

917 Figure S19: No CEACAM6 expression on human peripheral monocytes.

918 Supplementaal Method: Automated image analysis of *C. albicans* cells in kidney sections.
919 Development, evaluation and detailed results.

920 Supplementary Tables (XLSX file):

921 Supplementary Tables S1, S2, S3, S4, S5, and S6: Serum glycoproteome analyses.
922 Comparisons of glycoproteomes and pathway analysis of these comparisons, Tables S1, S2,
923 S3, S4, S5 and S6 relate to Figure 2b, 2c, 2g, 2h,2f, and 2i, respectively.

924 Supplementary Table S7: Protein groups (results of glycoproteome analysis).

925

926 **13 References**

927

928 1. Eggimann P, Pittet D. Candida colonization index and subsequent infection in
929 critically ill surgical patients: 20 years later. *Intensive Care Med* **40**, 1429-1448
930 (2014).

931

932 2. Lopes JP, Lionakis MS. Pathogenesis and virulence of Candida albicans. *Virulence* **13**,
933 89-121 (2022).

934

935 3. Lionakis MS. New insights into innate immune control of systemic candidiasis. *Med*
936 *Mycol* **52**, 555-564 (2014).

937

938 4. Goyal S, Castrillon-Betancur JC, Klaile E, Slevogt H. The Interaction of Human
939 Pathogenic Fungi With C-Type Lectin Receptors. *Front Immunol* **9**, 1261 (2018).

940

941 5. Bourgeois C, Kuchler K. Fungal pathogens-a sweet and sour treat for toll-like
942 receptors. *Front Cell Infect Microbiol* **2**, 142 (2012).

943

944 6. Klaile E*, et al.* Binding of Candida albicans to Human CEACAM1 and CEACAM6
945 Modulates the Inflammatory Response of Intestinal Epithelial Cells. *mBio* **8**, (2017).

946

947 7. Bonsignore P, Kuiper JWP, Adrian J, Goob G, Hauck CR. CEACAM3-A Prim(at)e
948 Invention for Opsonin-Independent Phagocytosis of Bacteria. *Front Immunol* **10**, 3160
949 (2019).

950

951 8. Tchoupa AK, Schuhmacher T, Hauck CR. Signaling by epithelial members of the
952 CEACAM family - mucosal docking sites for pathogenic bacteria. *Cell Commun*
953 *Signal* **12**, 27 (2014).

954

955 9. Heinrich A*, et al.* Moraxella catarrhalis induces CEACAM3-Syk-CARD9-dependent
956 activation of human granulocytes. *Cell Microbiol* **18**, 1570-1582 (2016).

957

958 10. Ambrosi C, Scribano D, Sarshar M, Zagaglia C, Singer BB, Palamara AT.
959 Acinetobacter baumannii Targets Human Carcinoembryonic Antigen-Related Cell
960 Adhesion Molecules (CEACAMs) for Invasion of Pneumocytes. *mSystems* **5**, (2020).

961

962 11. Javaheri A*, et al.* Helicobacter pylori adhesin HopQ engages in a virulence-enhancing
963 interaction with human CEACAMs. *Nat Microbiol* **2**, 16189 (2016).

964

965 12. Tegtmeyer N*, et al.* Type IV secretion of Helicobacter pylori CagA into oral epithelial
966 cells is prevented by the absence of CEACAM receptor expression. *Gut Pathog* **12**, 25
967 (2020).

968

969 13. Sarantis H, Gray-Owen SD. Defining the roles of human carcinoembryonic antigen-
970 related cellular adhesion molecules during neutrophil responses to Neisseria
971 gonorrhoeae. *Infect Immun* **80**, 345-358 (2012).

972

973 14. Klaile E*, et al.* Antibody ligation of CEACAM1, CEACAM3, and CEACAM6,
974 differentially enhance the cytokine release of human neutrophils in responses to
975 Candida albicans. *Cell Immunol* **371**, 104459 (2022).

976

977 15. Klaile E*, et al.* Unaltered Fungal Burden and Lethality in Human CEACAM1-
978 Transgenic Mice During Candida albicans Dissemination and Systemic Infection.
979 *Front Microbiol* **10**, 2703 (2019).

980

981 16. Hirai A*, et al.* Role of mouse hepatitis virus (MHV) receptor murine CEACAM1 in
982 the resistance of mice to MHV infection: studies of mice with chimeric mCEACAM1a
983 and mCEACAM1b. *J Virol* **84**, 6654-6666 (2010).

984

985 17. Zhang Z*, et al.* CEACAM1 regulates the IL-6 mediated fever response to LPS through
986 the RP105 receptor in murine monocytes. *BMC Immunol* **20**, 7 (2019).

987

988 18. Zoller J, *et al.* CEACAM1 regulates CD8(+) T cell immunity and protects from severe
989 pathology during Citrobacter rodentium induced colitis. *Gut Microbes* **11**, 1790-1805
990 (2020).

991

992 19. Zebhauser R, Kammerer R, Eisenried A, McLellan A, Moore T, Zimmermann W.
993 Identification of a novel group of evolutionarily conserved members within the rapidly
994 diverging murine Cea family. *Genomics* **86**, 566-580 (2005).

995

996 20. Chan CH, Stanners CP. Novel mouse model for carcinoembryonic antigen-based
997 therapy. *Mol Ther* **9**, 775-785 (2004).

998

999 21. Carvalho FA, *et al.* Crohn's disease adherent-invasive Escherichia coli colonize and
1000 induce strong gut inflammation in transgenic mice expressing human CEACAM. *J*
1001 *Exp Med* **206**, 2179-2189 (2009).

1002

1003 22. Denizot J, *et al.* Adherent-invasive Escherichia coli induce claudin-2 expression and
1004 barrier defect in CEABAC10 mice and Crohn's disease patients. *Inflamm Bowel Dis*
1005 **18**, 294-304 (2012).

1006

1007 23. Sintsova A, Guo CX, Sarantis H, Mak TW, Glogauer M, Gray-Owen SD. Bcl10
1008 synergistically links CEACAM3 and TLR-dependent inflammatory signalling. *Cell*
1009 *Microbiol* **20**, (2018).

1010

1011 24. Hebecker B, *et al.* Dual-species transcriptional profiling during systemic candidiasis
1012 reveals organ-specific host-pathogen interactions. *Sci Rep* **6**, 36055 (2016).

1013

1014 25. Jacobsen ID, Luttich A, Kurzai O, Hube B, Brock M. In vivo imaging of disseminated
1015 murine Candida albicans infection reveals unexpected host sites of fungal persistence
1016 during antifungal therapy. *J Antimicrob Chemother* **69**, 2785-2796 (2014).

1017

1018 26. Iba T, Umemura Y, Wada H, Levy JH. Roles of Coagulation Abnormalities and
1019 Microthrombosis in Sepsis: Pathophysiology, Diagnosis, and Treatment. *Arch Med*
1020 *Res* **52**, 788-797 (2021).

1021

1022 27. Lionakis MS, Lim JK, Lee CC, Murphy PM. Organ-specific innate immune responses
1023 in a mouse model of invasive candidiasis. *J Innate Immun* **3**, 180-199 (2011).

1024

1025 28. Thomas J, *et al.* CEACAMS 1, 5, and 6 in disease and cancer: interactions with
1026 pathogens. *Genes Cancer* **14**, 12-29 (2023).

1027

1028 29. Sonego F, *et al.* Paradoxical Roles of the Neutrophil in Sepsis: Protective and
1029 Deleterious. *Front Immunol* **7**, 155 (2016).

1030

1031 30. Metzemaekers M, Gouwy M, Proost P. Neutrophil chemoattractant receptors in health
1032 and disease: double-edged swords. *Cell Mol Immunol* **17**, 433-450 (2020).

1033

1034 31. Kuroki M, Yamanaka T, Matsuo Y, Oikawa S, Nakazato H, Matsuoka Y.
1035 Immunochemical analysis of carcinoembryonic antigen (CEA)-related antigens
1036 differentially localized in intracellular granules of human neutrophils. *Immunol Invest*
1037 **24**, 829-843 (1995).

1038

1039 32. Skubitz KM, Skubitz AP. Two new synthetic peptides from the N-domain of
1040 CEACAM1 (CD66a) stimulate neutrophil adhesion to endothelial cells. *Biopolymers*
1041 **96**, 25-31 (2011).

1042

1043 33. Skubitz KM, Skubitz AP. Interdependency of CEACAM-1, -3, -6, and -8 induced
1044 human neutrophil adhesion to endothelial cells. *J Transl Med* **6**, 78 (2008).

1045

1046 34. Wu X, *et al.* Human Liver Macrophage Subsets Defined by CD32. *Front Immunol* **11**,
1047 2108 (2020).

1048

1049 35. Baharom F, Rankin G, Blomberg A, Smed-Sorensen A. Human Lung Mononuclear
1050 Phagocytes in Health and Disease. *Front Immunol* **8**, 499 (2017).

1051

1052 36. Gray-Owen SD, Blumberg RS. CEACAM1: contact-dependent control of immunity.
1053 *Nat Rev Immunol* **6**, 433-446 (2006).

1054

1055 37. Behrens IK, *et al.* The HopQ-CEACAM Interaction Controls CagA Translocation,
1056 Phosphorylation, and Phagocytosis of Helicobacter pylori in Neutrophils. *mBio* **11**,
1057 (2020).

1058

1059 38. Martinez-Medina M, *et al.* Western diet induces dysbiosis with increased E coli in
1060 CEABAC10 mice, alters host barrier function favouring AIEC colonisation. *Gut* **63**,
1061 116-124 (2014).

1062

1063 39. Spellberg B, Ibrahim AS, Edwards JE, Jr., Filler SG. Mice with disseminated
1064 candidiasis die of progressive sepsis. *J Infect Dis* **192**, 336-343 (2005).

1065

1066 40. Lionakis MS*, et al.* Chemokine receptor Ccr1 drives neutrophil-mediated kidney
1067 immunopathology and mortality in invasive candidiasis. *PLoS Pathog* **8**, e1002865
1068 (2012).

1069

1070 41. Lionakis MS, Albert ND, Swamydas M, Lee CR, Loetscher P, Kontoyiannis DP.
1071 Pharmacological Blockade of the Chemokine Receptor CCR1 Protects Mice from
1072 Systemic Candidiasis of Hematogenous Origin. *Antimicrob Agents Chemother* **61**,
1073 (2017).

1074

1075 42. Yano J, Peters BM, Noverr MC, Fidel PL, Jr. Novel Mechanism behind the
1076 Immunopathogenesis of Vulvovaginal Candidiasis: "Neutrophil Anergy". *Infect*
1077 *Immun* **86**, (2018).

1078

1079 43. Souto FO*, et al.* Liver X Receptor Activation Impairs Neutrophil Functions and
1080 Aggravates Sepsis. *J Infect Dis* **221**, 1542-1553 (2020).

1081

1082 44. Wang YY*, et al.* Liver X receptor agonist GW3965 dose-dependently regulates lps-
1083 mediated liver injury and modulates posttranscriptional TNF-alpha production and p38
1084 mitogen-activated protein kinase activation in liver macrophages. *Shock* **32**, 548-553
1085 (2009).

1086

1087 45. Myhre AE*, et al.* Liver X receptor is a key regulator of cytokine release in human
1088 monocytes. *Shock* **29**, 468-474 (2008).

1089

1090 46. Ruiqi W*, et al.* Monocyte-derived macrophages contribute to the deterioration of
1091 immunological liver injury in mice. *Int Immunopharmacol* **124**, 111036 (2023).

1092

1093 47. Austermeier S, Kasper L, Westman J, Gresnigt MS. I want to break free - macrophage
1094 strategies to recognize and kill Candida albicans, and fungal counter-strategies to
1095 escape. *Curr Opin Microbiol* **58**, 15-23 (2020).

1096

1097 48. Smeekens SP*, et al.* The classical CD14(+)(+) CD16(-) monocytes, but not the
1098 patrolling CD14(+) CD16(+) monocytes, promote Th17 responses to Candida
1099 albicans. *Eur J Immunol* **41**, 2915-2924 (2011).

1100

1101 49. Ngo LY, Kasahara S, Kumasaka DK, Knoblaugh SE, Jhingran A, Hohl TM.
1102 Inflammatory monocytes mediate early and organ-specific innate defense during
1103 systemic candidiasis. *J Infect Dis* **209**, 109-119 (2014).

1104

1105 50. Langenhorst D*, et al.* Soluble Enolase 1 of Candida albicans and Aspergillus
1106 fumigatus Stimulates Human and Mouse B Cells and Monocytes. *J Immunol* **211**, 804-
1107 815 (2023).

1108

1109 51. Zhang X, Liu H, Hashimoto K, Yuan S, Zhang J. The gut-liver axis in sepsis:
1110 interaction mechanisms and therapeutic potential. *Crit Care* **26**, 213 (2022).

1111

1112 52. Xu S, Shinohara ML. Tissue-Resident Macrophages in Fungal Infections. *Front*
1113 *Immunol* **8**, 1798 (2017).

1114

1115 53. Lionakis MS*, et al.* CX3CR1-dependent renal macrophage survival promotes Candida
1116 control and host survival. *J Clin Invest* **123**, 5035-5051 (2013).

1117

1118 54. Strnad P, Tacke F, Koch A, Trautwein C. Liver - guardian, modifier and target of
1119 sepsis. *Nat Rev Gastroenterol Hepatol* **14**, 55-66 (2017).

1120

1121 55. Bauer M, Press AT, Trauner M. The liver in sepsis: patterns of response and injury.
1122 *Curr Opin Crit Care* **19**, 123-127 (2013).

1123

1124 56. MacCallum DM, Castillo L, Brown AJ, Gow NA, Odds FC. Early-expressed
1125 chemokines predict kidney immunopathology in experimental disseminated Candida
1126 albicans infections. *PLoS One* **4**, e6420 (2009).

1127

1128 57. Bloos F, Reinhart K. Rapid diagnosis of sepsis. *Virulence* **5**, 154-160 (2014).

1129

1130 58. Honda S*, et al.* Marginal zone B cells exacerbate endotoxic shock via interleukin-6
1131 secretion induced by Fcalpha/muR-coupled TLR4 signalling. *Nat Commun* **7**, 11498
1132 (2016).

1133

1134 59. Drummond RA, Lionakis MS. Organ-specific mechanisms linking innate and adaptive
1135 antifungal immunity. *Semin Cell Dev Biol* **89**, 78-90 (2019).

1136

1137 60. Drummond RA. What fungal CNS infections can teach us about neuroimmunology
1138 and CNS-specific immunity. *Semin Immunol* **67**, 101751 (2023).

1139

1140 61. Drummond RA*, et al.* CARD9(+) microglia promote antifungal immunity via IL-
1141 1beta- and CXCL1-mediated neutrophil recruitment. *Nat Immunol* **20**, 559-570
1142 (2019).

1143

1144 62. Gil ML, Gozalbo D. Role of Toll-like receptors in systemic Candida albicans
1145 infections. *Front Biosci (Landmark Ed)* **14**, 570-582 (2009).

1146

1147 63. Taylor PR*, et al.* Dectin-1 is required for beta-glucan recognition and control of fungal
1148 infection. *Nat Immunol* **8**, 31-38 (2007).

1149

1150 64. Burtin P, Quan PC, Sabine MC. Nonspecific cross reacting antigen as a marker for
1151 human polymorphs, macrophages and monocytes. *Nature* **255**, 714-716 (1975).

1152

1153 65. Bordes M, Knobel S, Martin F. Carcinoembryonic antigen (CEA) and related antigens
1154 in blood cells and hematopoietic tissues. *Eur J Cancer (1965)* **11**, 783-786 (1975).

1155

1156 66. Nap M*, et al.* Specificity and affinity of monoclonal antibodies against
1157 carcinoembryonic antigen. *Cancer Res* **52**, 2329-2339 (1992).

1158

1159 67. Gerst R, Cseresnyes Z, Figge MT. JIPipe: visual batch processing for ImageJ. *Nat*
1160 *Methods* **20**, 168-169 (2023).

1161

1162 68. Muller MM*, et al.* Global analysis of glycoproteins identifies markers of endotoxin
1163 tolerant monocytes and GPR84 as a modulator of TNFalpha expression. *Sci Rep* **7**,
1164 838 (2017).

1165

1166 69. Cox J, Mann M. MaxQuant enables high peptide identification rates, individualized
1167 p.p.b.-range mass accuracies and proteome-wide protein quantification. *Nat*
1168 *Biotechnol* **26**, 1367-1372 (2008).

1169

1170 70. Tyanova S*, et al.* The Perseus computational platform for comprehensive analysis of
1171 (prote)omics data. *Nat Methods* **13**, 731-740 (2016).

1172

1173 71. Benjamini Y, Drai D, Elmer G, Kafkafi N, Golani I. Controlling the false discovery
1174 rate in behavior genetics research. *Behav Brain Res* **125**, 279-284 (2001).

1175

1176 72. Perez-Riverol Y*, et al.* The PRIDE database at 20 years: 2025 update. *Nucleic Acids*
1177 *Res* **53**, D543-d553 (2025).

1178

1179